

An experimental study of gypsum dissolution coupled to CaCO₃ precipitation and its application to carbon storage

Lei Yu^{a,b}; Leyla M. Daniels^b, Josephina J.P.A. Mulders^b, Giuseppe D. Saldi^{b,d}; Anna L. Harrison^{b,c}, Li Liu^a, Eric H. Oelkers^{b,d*}

a. College of Earth Sciences, Jilin University, 130061 Changchun, P. R. China

b. Department of Earth Sciences, University College London, Gower Street, WC1E 6BT London, United Kingdom

c. Department of Geological Sciences and Geological Engineering and the School of Environmental Studies, Queen's University, Kingston, Ontario, K7L 3N6 Canada

d. GET-Université de Toulouse-CNRS-IRD-OMP, 14 Avenue Edouard Belin, 31400 Toulouse, France

ABSTRACT

Coupled gypsum dissolution-calcium carbonate precipitation experiments were performed in closed system reactors and in the presence of either aqueous 0.1 M Na₂CO₃, 0.1 M NaHCO₃ or 0.1 M Na₂CO₃ + 0.2 M NaOH solutions. Gypsum dissolved immediately at the start of each experiment provoking the precipitation sequentially of vaterite, calcite and trace aragonite. Fine-grained amorphous carbon carbonate may also be present shortly after each experiment began. Each experiment approached equilibrium within 119 h leading to the maximum possible transformation of gypsum to calcite over this time frame. The rapid transformation of gypsum to calcite in these experiments suggests a similar rapid transformation of gypsum or anhydrite into calcite could occur during subsurface carbon storage efforts where evaporites are present. Evaporite deposits could thus potentially be used for carbonation if sufficient alkalinity is available to neutralize the acid liberated by the gypsum carbonation reaction. Due to a negative volume of the gypsum or anhydrite to calcite transformation, however, the carbonation of these minerals will potentially damage the integrity of evaporite caprocks.

1. INTRODUCTION

This study is focused on the mineralization of water dissolved carbon-dioxide through its interaction with gypsum. The mineralization of CO₂ or ‘mineral carbonation’ is the process by which CO₂ is transformed into stable carbonate minerals through its reaction with divalent cations, such as Ca²⁺, Mg²⁺, and Fe²⁺, sourced from non-carbonate minerals (Lackner et al 1995; Oelkers et al., 2008; Power et al. 2013). A large number of past studies have focused on quantifying various aspects of mineral carbonation as a means of carbon storage (Bachu et al., 1994; Gunter et al., 1997; Johnson et al., 2001; Baines and Worden, 2004; Oelkers and Schott, 2005; McGrail et al., 2006; Goldberg et al., 2008, 2018; Oelkers and Cole, 2008; Oelkers et al., 2008; Flaathen et al., 2009; Schaef et al., 2009; Wakahama et al., 2009; Matter et al., 2011, 2016; Wolff-Boenisch et al., 2011; Gislason and Oelkers, 2014;).

Calcite is most the abundant carbonate mineral near the Earth’s surface and it is particularly favorable for a mineralogical carbon-dioxide host due to its stability and rapid precipitation kinetics (Palandri and Kharaka, 2004; Matter et al., 2011; Snæbjörnsdóttir et al., 2017). Two minerals that can readily provide Ca for the formation of calcite are gypsum (CaSO₄·2H₂O) and anhydrite (CaSO₄). Gypsum and anhydrite are common minerals in evaporite deposits (Spencer, 2000). Compared to many siliciclastic formations, evaporite layers tend to have a lower intrinsic permeability and a higher CO₂ breakthrough pressure (Hangx et al., 2010) and do not dissolve in direct response to CO₂-generated acidity (Smith et al., 2012). As such, evaporite layers are considered to be effective as caprocks and can thus enhance the security of subsurface geologic carbon storage. In the presence of carbonate-bearing aqueous fluids at more alkaline conditions, however, these minerals are susceptible to dissolve and transform into carbonate minerals (Stafford et al., 2008). Such a transformation has the potential to increase the porosity of evaporite layers allowing CO₂ to leak back to the atmosphere.

Basalts and ultramafic rocks are commonly considered as the target host rocks for subsurface mineral carbonation (McGrail et al., 2006; Goldberg et al., 2008; Gislason

et al., 2010; Gislason and Oelkers, 2014; Goldberg et al., 2018; Snæbjörnsdóttir et al., 2018; Oelkers et al., 2019). There are several advantages in storing CO₂ in basaltic and ultramafic rocks. However, when the basaltic rocks are first dissolved in CO₂-rich, sulfate-bearing acid brines, such as seawater, the Ca released from the dissolving basalt could readily combine with SO₄²⁻ in the seawater and precipitate gypsum or anhydrite (Garcia et al., 2011). Indeed, gypsum and/or anhydrite could readily form during the initial stages of the injection of CO₂-rich seawater into sub-seafloor basalts (Voigt et al., 2018). This process would consume the Ca released from basalts limiting the amount of Ca available for carbonate mineral precipitation (Ruiz-Agudo et al., 2015). The formation of gypsum and/or anhydrite can also dramatically reduce the porosity of target carbon storage reservoirs (Ahr, 2008) and could clog injection wells (Rendel et al., 2016). The quantification of the rates and extent of the transformation between gypsum or anhydrite and calcite could be essential to determining the viability of numerous subsurface carbon storage sites.

This study is focused on the dissolution of gypsum coupled to calcium carbonate precipitation. Gypsum dissolution rates measured in the laboratory suggest this reaction is rapid and will readily approach equilibrium with the aqueous phase (Jeschke et al., 2001; Colombani and Bert, 2007; Tang et al., 2018). A number of studies have thus considered the carbonation of gypsum as a means for ex-situ carbon capture and storage (Lee et al., 2012; Azdarpour et al., 2014; Pérez-Moreno et al., 2015; González-Illanes et al., 2017; Tan et al., 2017; Rahmani, 2018; Seo et al., 2018). For example, Fernández-Díaz et al. (2009) reported the formation of amorphous calcium carbonate (ACC), vaterite, aragonite and calcite on the surface of gypsum (010) surfaces during its interaction with Na₂CO₃ bearing aqueous fluids. Roncal-Herrero et al. (2017) reported the precipitation of calcite and vaterite crystals on the surfaces of anhydrite during its interaction with Na₂CO₃ bearing aqueous fluids. This study builds upon these past works by quantifying the rates and extent of gypsum transformation to calcite as a function of fluid composition.

2. THEORETICAL BACKGROUND

The standard state adopted in this study is that of unit activity of pure minerals, and H₂O at any temperature and pressure. For aqueous species, the standard state is unit activity of the species in a hypothetical one molal solution referenced to infinite dilution at any temperature and pressure. All thermodynamic calculations reported in this study were performed using PHREEQC V3 (Parkhurst and Appelo, 2013) together with its llnl thermodynamic database (Johnson et al., 2000). The solubility products (K_{sp}) for amorphous calcium carbonate (ACC, $\log K_{sp} = -6.393$, Brečević and Nielsen, 1989) and vaterite ($\log K_{sp} = -7.913$, Rodriguez-Navarro et al., 2015) were added to this database prior to its use in calculations.

This study was designed to assess the rates and mechanism of the transformation of gypsum to calcite in the presence of aqueous carbonate. The dissolution of gypsum can be described by:



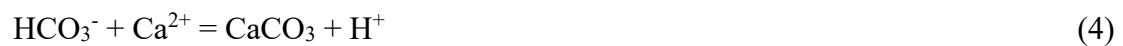
Taking account of the standard state, the law of mass action for this reaction is given by:

$$K_{gypsum} = a_{\text{Ca}^{2+}} a_{\text{SO}_4^{2-}} \quad (2)$$

where K_{gypsum} stands for the equilibrium constant of reaction (1), and a_i represents the activity of the subscripted aqueous species. The saturation state of an aqueous fluid with respect to gypsum can be quantified using the saturation index (SI_{gypsum}) defined by:

$$SI_{gypsum} = \log \left(\frac{IAP_{gypsum}}{K_{gypsum}} \right) \quad (3)$$

where IAP_{gypsum} signifies the aqueous ion activity product for reaction (1). Note that SI is negative when the fluid is undersaturated, positive when supersaturated, and zero at fluid-mineral equilibrium. The dissolution of gypsum adds calcium to the aqueous solution, which can provoke the precipitation of calcium carbonate phases (CaCO₃) if dissolved carbonate is present from:



Combining Eqn. (1) and (4) yields:



The degree to which reaction (5) converts gypsum to calcite depends strongly on pH. The concentration of dissolved calcium in equilibrium with gypsum at a total dissolved SO_4^{2-} concentration of 0.01 mol/kg and in equilibrium with calcite at atmospheric CO_2 pressure and 30 bars CO_2 pressure as a function of pH are illustrated in Fig. 1. Figure 1 was calculated using PHREEQC V3 (Parkhurst and Appelo, 2013) by setting alternatively the partial pressure of CO_2 in the input file to the partial pressure of interest, and balancing the charge of the fluid phase with either Na or Cl. Gypsum solubility is independent of both pH and CO_2 partial pressure, whereas the solubility of calcite is strongly pH dependent. At atmospheric CO_2 pressure and pH less than ~7.5, reaction (5) will tend to the left dissolving calcite and driving the precipitation of gypsum. Whereas if the pH of the fluid is greater than 7.5, gypsum would dissolve provoking the precipitation of calcite. Similarly, at a CO_2 pressure of 30 bars, reaction (5) will tend to the right dissolving gypsum and driving the precipitation of calcite at $\text{pH} > 5.1$. It can thus be anticipated that the presence of dissolved carbonate at basic conditions would tend to favor the formation of calcite from gypsum.

3. MATERIALS AND METHODS

Two kinds of gypsum were used in the experiments as starting solids. One was synthetic, analytical grade $\text{CaSO}_4 \cdot 2\text{H}_2\text{O}$ produced by Acros organics with a reported purity of more than 98%. This synthetic gypsum was used for experiment SYN11. The other consisted of natural gem-quality translucent crystals. This natural gypsum was used for experiments NAT8-1, NAT8-2, NAT11, NAT13 and the experimental series S8 and S11. The natural gypsum was ground with an agate mortar and pestle. Both the synthetic and natural gypsum powders were ultrasonically cleaned 5 times in ethanol to remove ultra-fine particles then dried in a desiccator at ambient temperature for one week. Following drying, both synthetic and natural gypsum samples were analyzed using an X'Pert PRO X-ray diffractometer (XRD) and a JSM-6480LV scanning electron microscope (SEM). X-ray diffractograms of the solids indicated the presence

of only well-crystallized gypsum (Fig. 2a). SEM images of these powers showed the gypsum surfaces to be smooth and fine-particle free (see Fig. 3a-d). The specific surface area of the synthetic gypsum and natural gypsum were $4.67 \pm 0.4 \text{ m}^2/\text{g}$ and $0.75 \pm 0.07 \text{ m}^2/\text{g}$ respectively, as determined by 10-point N_2 adsorption analysis, according to the BET method (Brunauer et al., 1938). The total inorganic carbon content of these solids was determined using a Thermo Flash EA 1112 Carbon/Nitrogen analyzer with a precision better than 0.1%.

Two types of experiments were run to study the transformation of gypsum to calcite. Experiments NAT8-1, NAT8-2, SYN11, NAT11 and NAT13 were performed in 250 mL Azlon polypropylene batch reactors with airtight lids. These lids were fitted with outlets allowing fluid sampling from the reactor during the experiments. Regular fluid sampling allowed tracking of the temporal evolution of the chemical composition of the fluid phase. Further experiments, experimental series S8 and S11, were performed in sealed 70 mL Nalgene polypropylene vials. These series consisted of 7 to 12 individual batch experiments with the same initial fluid and gypsum but run over different durations. These vials did not contain outlets for fluid sampling; each vial was sealed and opened only at the end of each individual batch experiment. At this time, all the fluid and solid was collected from the individual reactor. This allowed for the detailed characterization of the morphology and mineralogy of the solids as a function of time. Two types of fluid/solid mixing methods were used. Experiments NAT8-1 and SYN11 were continuously stirred with floating Teflon-coated magnetic stir bars. Whereas experiments NAT8-2, NAT11 and NAT13, and the experimental series S8 and S11 were run in shaking thermostatic water baths. All experiments were performed at a temperature of $25 \pm 1.5 \text{ }^\circ\text{C}$ and ambient pressure ($\sim 1 \text{ bar}$).

All experiments were initiated by adding a selected mass of ground, cleaned gypsum powder into the reactor containing an initial reactive aqueous fluid. All initial fluids were made using ultrapure de-ionized water ($18.2 \text{ M}\Omega \cdot \text{cm}$) together with Merck reagent grade Na_2CO_3 , NaHCO_3 and NaOH . The mass of gypsum used, the composition of all initial reactive aqueous fluids, and other experimental details are provided in Table 1.

The experiments in this study ran for up to 336 h. Between 1.5 and 2.0 g of fluid were sampled regularly from each of the 250 mL Azlon polypropylene batch reactors. These fluids as well as those from the individual batch reactors were sampled using polypropylene syringes equipped with 0.22 μm polyethersulfone filters, then separated into two subsamples; one subsample was used for measuring pH and alkalinity, the other was acidified with double distilled, ultrapure HNO_3 (to 2% HNO_3) for Ca and S analysis. The pH of these fluids was measured immediately after sampling using a Mettler Toledo F20 pH meter equipped with a LE438 Mettler Toledo electrode. The alkalinity of the fluid samples from all experiments were measured using a Mettler Toledo G10S automatic titrator equipped with a DGi115-SC electrode. Before each use, the electrodes for pH and alkalinity analyses were calibrated using NIST 4.01, 7.00, and 9.21 pH buffer solutions at 25 $^\circ\text{C}$. The uncertainties of measurements are ± 0.03 based on replicate analyses of the standard buffer solutions. The dissolved Ca and S were analyzed by inductively coupled plasma optical emission spectroscopy (ICP-OES) with a Varian 720. The detection limit was calculated to be 1.25×10^{-6} mol/kg for Ca and 1.34×10^{-6} mol/kg for S; the analytical uncertainty was generally lower than 5%. The total dissolved inorganic carbon (DIC) and the saturation state of the sampled fluids with respect to selected solid phases were calculated from measured pH, alkalinity, and Ca and S concentration using PHREEQC V3 ([Parkhurst and Appelo, 2013](#)). The post-experiment solids were collected via vacuum filtration with 0.22 μm nylon membrane filters. All solids were stored in a desiccator for ~ 1 week at ambient temperature prior to analysis.

As the initial fluids in the experiments performed in this study were essentially Ca and S free, the total mass of CaCO_3 precipitated ($m_{\text{CaCO}_3, \text{precipitated}}$) at any time during each experiment can be calculated from mass balance constraints taking account reactions 1 and 5 using:

$$m_{\text{CaCO}_3, \text{precipitated}} = m_S - m_{\text{Ca}} \quad (6)$$

where m_S and m_{Ca} refer to the total aqueous fluid mass in the reactor of S and Ca. The weight percent of CaCO_3 in the solid at any time ($\% \text{CaCO}_3$) is therefore

$$\%CaCO_3 = \frac{M_{CaCO_3}(m_S - m_{Ca})}{M_{CaCO_3}(m_S - m_{Ca}) + M_{Gypsum}(m_{Gypsum,initial} - m_S)} \quad (7)$$

where M_{CaCO_3} and M_{Gypsum} represent the molar weight of $CaCO_3$ and gypsum, respectively, and $m_{gypsum,initial}$, refers to the mass of gypsum in the reactor at the beginning of the experiment. Such calculations will be used in this study to assess the mineralogical evolution of the solids during the experiments presented below.

The maximum percent of gypsum transformed to $CaCO_3$ is limited by the initial masses of gypsum and dissolved carbonate in the closed system reactors. If all the dissolved carbonate initially present in the reactor is incorporated into $CaCO_3$ solids, and the aqueous Ca concentration is negligible compared to that in the solid phase, then the mass of gypsum remaining in the reactor at the completion of the reaction ($m_{gypsum\ remaining}$) would be:

$$m_{gypsum\ remaining} = (m_{gypsum,initial} - m_{carbonate,initial}) \quad (8)$$

then the maximum weight ratio of $CaCO_3$ (wt. %) in the solid phase would then be

$$\%CaCO_{3,max} = \frac{m_{carbonate,initial} M_{CaCO_3}}{m_{carbonate,initial} M_{CaCO_3} + (m_{gypsum,initial} - m_{carbonate,initial}) M_{gypsum}} \times 100\% \quad (9)$$

where $m_{carbonate,initial}$ and $m_{gypsum,initial}$ refer to total mass of dissolved carbonate and gypsum initially present in the closed system reactor, respectively. Note that the results for calcite mass ratio, deduced by Eqn. (9) will be limited somewhat by the solubility of $CaCO_3$ phases in the reactor fluid as some dissolved carbonate will remain in the fluid.

4. RESULTS

4.1. Chemical evolution of the fluid phase

4.1.1 Experiments performed in initial 100 mmol/kgw Na_2CO_3 solutions

The SYN11, NAT11 and S11 experiments were performed by exposing the initial natural or synthetic gypsum to an aqueous 0.1 M Na_2CO_3 solution. The chemical evolution of the fluid during these experiments is reported in Table 2 and shown in Fig.

The initial fluid pH of the SYN11 experiment was 11.36. The pH of this fluid decreased to 8.63 after only 0.08 h, then continued to decrease to an approximately constant value in the 8.04 to 8.42 range. The dissolved S concentration increased to 107 mmol/kgw during the first 0.08 h of the experimental series then remained close to constant, ranging from 90 to 109 mmol/kgw throughout the rest of the experiment. The aqueous Ca concentration remained close to constant ranging from 10.2 to 11.1 mmol/kgw after 0.42 h through the end of the experiment (Fig. 4a).

There was a distinctly slower gypsum dissolution rate in experiment NAT11 (Fig. 4b). The aqueous fluid had an initial pH of 11.11. This pH decreased to 10.77 during the first 22.8 h of reaction, and continued to decrease to 8.10 after 118.8 h. The pH subsequently remained relatively stable between 8.10 and 7.77 for the duration of the experiment. The aqueous S concentration increased to 88 mmol/kgw during the first 94.8 h of the experiment then remained relatively stable ranging from 100 and 116 mmol/kgw during the rest of the experiment. The measured aqueous Ca concentration remained relatively low compared to the corresponding aqueous S concentration throughout the experiment, and never exceeded 10.6 mmol/kgw. The alkalinity at the end of experiment was 1.74 mmol/kgw (Table 2). The calculated saturation indices of the final fluid with respect to gypsum, calcite, vaterite, aragonite and ACC were 0.14, 0.24, -0.38, 0.09 and -1.91, respectively, suggesting that the transformation between gypsum and the CaCO_3 phases occurred at near to equilibrium conditions (Fig. 7).

The pH of the original reactive aqueous solutions during experimental series S11, which consisted of a set of individual batch experiments run for a selected duration of time, is listed in Table 1 and ranged from 11.29 to 11.42. This pH remained in the range of 11.17 to 11.27 for the experiments having elapsed times of less than 2 h. The pH of the fluid samples collected from the experiments after 24 h of reaction decreased to 6.97 and the pH remained within the range 6.74 and 7.87 for the remainder of this experimental series (Fig. 4c). The reactive fluid S and Ca concentrations increased substantially at the beginning of these experiments. After 24 h of reaction, the dissolved S concentrations ranged from 119 to 130 mmol/kgw, while the dissolved Ca concentrations ranged from 8.8 to 10.4 mmol/kgw. Similarly, the measured alkalinities

decreased to 3 from 100 mmol/kgw over the first 24 h (see Fig. 4c), then remained within the range from 1.7 to 2.1 mmol/kgw during the rest of the experimental series. The calculated saturation indices for calcite, vaterite and aragonite showed that these phases were supersaturated during the first 24 h of the experimental series (Fig. 7). In contrast, the reactive fluid was undersaturated with respect to gypsum during the first 24 h of the experiments, but was at equilibrium with gypsum thereafter. Moreover, ACC was calculated to be undersaturated in all collected fluid samples.

4.1.2 Experiments performed in initial 100 mmol/kgw NaHCO₃ aqueous solutions

The results of experiments NAT8-1 and NAT8-2, and the S8 experimental series, which were begun by placing gypsum into 0.1 mol/kgw aqueous NaHCO₃ solutions, are summarized in Table 3 and shown in Fig. 5.

In experiment NAT8-1, the initial fluid pH was 8.41; the pH dropped to 7.40 within 0.17 h of reaction. With more reaction time, the pH decreased further, attaining a near to constant value ranging from 6.76 to 7.15. During the first 0.17 h of the reaction, aqueous S and Ca concentration increased to 22.75 mmol/kgw and 18.31 mmol/kgw respectively. Subsequently, the aqueous S concentration increased while the aqueous Ca decreased. The S and Ca concentrations trended to near constant values after 46.6 h ranging from 36.8 to 43.1 mmol/kgw and from 12.6 to 13.7 mmol/kgw, respectively (Fig. 5a).

The NAT8-2 experiment exhibited a similar evolution as the NAT8-1 experiment (Fig. 5b). The fluid pH dropped from an initial value of 8.42 to 7.11 during the first 0.1 h of the experimental series then subsequently ranged from 6.85 to 6.99 for the rest of the series. Within the first 0.1 h of the experimental series, the S and Ca concentrations in the reactive fluid increased to 23 mmol/kgw and 19 mmol/kgw respectively. The S concentration continued to increase with time reaching 38 mmol/kgw at 22.3 h, while the Ca concentration decreased to 13 mmol/kgw by this time. Subsequently these concentrations remained approximately constant. The reactive fluid was close to saturation with respect to gypsum and the CaCO₃ phases during this steady-state period. The saturation indices were calculated to be 0.02, 0.98, 0.41, 0.84 and -1.11 for gypsum,

calcite, vaterite, aragonite and ACC, respectively, at the end of the experiment (see Fig. 7).

The results of the S8 series are provided in Table 3 and Fig. 5. The original pH of these reactive fluids was between 8.05 and 8.41 (Table 1). The fluid pH decreased to 6.74 during the first 24.3 h reaction then remained in the range of 6.53 to 6.76 thereafter (Fig. 5c). Similarly, the aqueous fluid S and Ca concentrations increased during the early part of the experimental series, before settling in a range of 39.2 to 42.7 mmol/kgw for S and 13.7 to 13.9 mmol/kgw for Ca after 71.9 h. Calculated alkalinities decreased continuously with time as CaCO_3 phases continue to precipitate (Table 3). The saturation indices of these fluids with respect to selected minerals are depicted in Fig. 7 and tabulated in Table 3. Vaterite is found to be strongly supersaturated during the first 24 h of reaction, whereas ACC was undersaturated throughout the experiments. The fluids were close to saturation with respect to gypsum after 24 h of reaction, whereas calcite and aragonite were calculated to be slightly undersaturated.

4.1.3 Experiments performed in initial 100 mol/kgw Na_2CO_3 + 200 mol/kgw NaOH aqueous solutions

The initial fluid for the NAT13 experiment was an aqueous 100 mmol/kgw Na_2CO_3 and 200 mmol/kgw NaOH solution. The results of this experiment are provided in Table 4 and Fig. 6. The initial pH of this solution was 12.86 and remained within the range 12.64 and 13.10 throughout the experiment. Both the reactive fluid S and Ca increased during the first 45.4 h of the experiment then remained close to constant. After this time, the dissolved S concentrations ranged from 120 to 125 mmol/kgw whereas the dissolved Ca concentrations ranged from 5 to 8.5 mmol/kgw. At the end of this experiment, the pH and reactive fluid alkalinity were 12.97 and 158 mmol/kgw respectively (Table 4). The calculated DIC was 1.38 mmol/kgw and the calculated saturation indices in the fluid with respect to gypsum, calcite, vaterite, aragonite and ACC were 0.74, 2.17, 2.03, 1.60 and 0.08, respectively, at the end of the experiment (Table 4, Fig. 7).

4.2. Compositions of recovered solids

X-ray diffraction (XRD) patterns were obtained from all initial and collected reacted solids. A number of representative XRD patterns are shown in Fig. 2. XRD patterns of the unreacted natural and synthetic show the solids to be pure gypsum without any carbonates or other phases present (Fig. 2a). In the solids recovered after 0.2 h in the experimental series S11 (sample S11-1), small peaks indicative of vaterite and calcite are observed (Fig. 2b). The XRD patterns of solids recovered after 24.1 h and 167.8 h of this experimental series show the vaterite and calcite peaks becoming more apparent, while the gypsum peaks decreased in magnitude (Fig. 2c, d). The XRD pattern of the final sample recovered from this experimental series, S11-12, after 336 hours of reaction shows that the calcite peaks are dominant while only small peaks for gypsum and aragonite could be detected (Fig. 2e), hence the dominant mineral in the solid collected is calcite rather than gypsum.

Scanning electron microscope images of the solids collected from experiments having a 1.0 h, 2.0 h and 336 h reaction duration from the S11 series are presented in Fig. 8a - h. Within 2.0 h after the start of the experimental series, a large number of semi-spherical calcium carbonate grains with the sizes of 2.3 to 3.5 μm formed on the surface of gypsum (Fig. 8a). These grains are associated with irregularly shaped etch pits on the gypsum (Fig. 8b, d). It is plausible that the formation of this carbonate locally lowered the concentration of Ca in the fluid phase promoting localized rapid dissolution of gypsum and formation of these etch pits. With additional reaction time, it can be seen that calcite and vaterite crystals grew on the gypsum surface (Fig. 8b - h).

The measured CaCO_3 contents for recovered solids are in a good agreement with the corresponding CaCO_3 contents calculated from Eqn. (7) and the reactor fluid compositions. The measured CaCO_3 contents listed in Table 5 indicate the final CaCO_3 contents of the recovered solids are 73.3, 11.6 and 73.5 wt. % for experiments NAT11, NAT8-2 and NAT13, respectively (see Fig. 8). In total, these experiments fixed 0.32, 0.05 and 0.32 g CO_2/g solid (Table 5). The calculated CaCO_3 contents determined from fluid compositions by using Eqn (7), indicate that CaCO_3 precipitated immediately as the experiment started, and most CaCO_3 precipitated within first few days of each

experiment (see Fig. 9). In the experiments performed in 100 mmol/kgw Na_2CO_3 (experiment NAT11), almost all of the CaCO_3 formed between 0 and 118.8 h, and precipitation stopped almost completely thereafter (Fig. 9a). In total, the calculated mass fraction of CaCO_3 in the solid was 76.2 wt. % following the completion of the reaction for the experiment NAT11 (Table 5). In the experiments performed in aqueous 100 mmol/kgw NaHCO_3 solutions (experiment NAT8-2), the CaCO_3 mainly formed during the first 22.3 h. In total, the calculated CaCO_3 precipitated in the solids at the end of NAT8-2 was 15.3 wt. % (Table 5 and Fig. 9b), In the experiments performed in an aqueous 100 mmol/kgw Na_2CO_3 + 200 mmol/kgw NaOH solution, experiment NAT13, the carbonates mainly precipitated during the first 45.4 h of the experiment, then essentially stopped after the calculated mass fraction of CaCO_3 in the solid was 83.5 wt. % (Table 5 and Fig. 9c). Note that in all cases the final mass of CaCO_3 precipitated was limited by the relative mass of gypsum compared to dissolved carbonate originally in the reactors. This is evident in Fig 9, which also plots the maximum gypsum to calcite conversion percent in each experiment. If all the dissolved carbonate could transform into calcite and precipitated from the fluid, the calculated maximum mass fraction of CaCO_3 in the solids would be 77.5, 12.3 and 82.6 wt. % for NAT11, NAT8-2 and NAT13 respectively (Fig. 8). In all cases, the mass fractions of CaCO_3 approach their maximum gypsum to carbonate conversions (Fig. 9a, c).

5. DISCUSSION

5.1. Mineralogical evolution during the carbonation process

The observations summarized above indicate that the carbonation of gypsum began by the initial formation of either fine grained amorphous calcium carbonate, or vaterite, followed by calcite and by aragonite in some of the experiments (see Fig. 8). Note that ACC was undersaturated in the reactive solutions during all experiments except in the final NAT13 fluid samples, whose *SI* of ACC was 0.08 (Table 4). Due to the small size and mass of the initial grains, however, it was not possible to unambiguously determine the identity of these grains. Nevertheless the formation of ACC on dissolving gypsum surfaces when the bulk fluids are undersaturated with

respect to ACC is consistent with the conclusions of [Fernández-Díaz et al. \(2009\)](#) who proposed that such observations could stem from the sluggish transport of aqueous Ca away from this surface relative to the fast dissolution rates. ACC often forms immediately after the mixture of Ca^{2+} and CO_3^{2-} in aqueous solution ([Sawada, 1997](#)). ACC was also the first product reported to be observed during the carbonation of lime ([Moorehead, 1986](#); [Cizer et al., 2012a](#); [2012b](#); [Santos et al., 2013](#); [Song et al., 2014](#)). As the reaction time increased in all experiments, the minute grains transform into larger CaCO_3 polymorphs similar to the observations of [Bolze et al. \(2002\)](#), [Pontoni et al. \(2003\)](#) and [Rodríguez-Blanco et al. \(2011\)](#). According to the XRD results for experiment S11-1, vaterite and calcite formed on the gypsum surface after 0.20 h reaction time (Fig. 2b). In the two solid samples collected after 24.1 and 167.8 hours of reaction (Fig. 2c, d), vaterite and calcite became more dominant, while gypsum continued to dissolve. After 336 h of reaction, vaterite decreased in abundance, and SEM images, such as shown in Fig. 8g - h, indicate that vaterite transformed into calcite. These images showed a close proximity between dissolving vaterite and growing calcite similar to what might be found for a coupled dissolution-precipitation mechanism ([Putnis, 2009](#)). In the sample collected from the 336 h experiment, aragonite peaks were detected in the XRD diffractogram (Fig. 2e) despite calcite being more stable than aragonite at 25 °C. Previous experimental results have reported aragonite formation during the carbonation of gypsum or anhydrite at ~25 °C ([Spanos and Koutsoukos, 1998](#); [Fernández-Díaz et al., 2009](#); [Atree-Williams et al., 2017](#)). Field studies have also reported the formation of aragonite as a replacement product of gypsum in both the sediments of the Upper Permian Zechstein Group of Central Germany ([Peckmann et al., 1999](#)) and the lacustrine deposits of the Miocene Teruel and Cabriel Basins in eastern Spain ([Anadón et al., 1992](#)). [Bischoff and Fyfe \(1968\)](#) and [Bischoff \(1968\)](#) found that high aqueous SO_4^{2-} concentrations could inhibit calcite formation favoring aragonite. Moreover, aragonite tends to nucleate in calcium limited or high dissolved carbonate concentration conditions ([Given and Wilkinson, 1985](#); [Fernández-Díaz et al., 1996](#)).

5.2. Impacts of mixing method and gypsum surface area on the carbonation rate

The experiments of this study were run using two distinct mixing methods – magnetic stirring bars and shaking in a thermostatic bath. The effect of the stirring method on gypsum carbonation rates can be evaluated by comparing the results of experiments NAT8-1 and NAT8-2 (Fig. 5a and 5b). Both experiments dissolved natural gypsum in 0.1 mol/kgw NaHCO₃ solutions but used different mixing methods. The temporal evolution of the reactive fluid S and Ca concentration was almost identical between these two experiments. Both attained approximately equilibrium fluid concentrations within ~24 h. Thereafter the Ca concentrations of the fluid phases in both experiments ranged between 12.0 and 16.9 mmol/kgw and the S concentrations range between 36.7 and 43.1 mmol/kgw (see Table 3). According to the experimental results in this study, the normalized dissolution rate constant of gypsum during its carbonation is $1.1 \pm 0.1 \times 10^{-7}$ mol/m²/s in both experiments (see section 5.3). It follows that the choice of mixing method has no apparent effect on rate and extent of the gypsum-to-calcite. The consistency of these results suggests their generality and their potential applicability to assessing gypsum carbonation in natural systems.

The effect of surface area on gypsum carbonation rates can be assessed by comparing the results of experiments SYN11 and NAT11 combined with S11 series, which are presented in Fig. 4a and 4b, respectively. Note that the dissolution of synthetic gypsum was nearly instantaneous and that the fluid achieved close to equilibrium conditions with respect to gypsum 0.42 h after the start of the reaction in the SYN11 experiment (Fig. 4a). In the NAT11 experiment, which reacted natural gypsum with lower specific surface area than the synthetic gypsum used in SYN11, an equilibrium state was not attained until after 71.9 to 94.8 h of reaction (Fig 4b). These results are consistent with previous work showing that the dissolution rate of gypsum is controlled primarily by its surface area and Ca concentration in the reactive fluid (Christoffersen and Christoffersen, 1976; Liu and Nancollas, 1971; Feng et al., 2017; Tang et al., 2018). Note that despite the difference in dissolution rates, the final reactive fluid Ca and S concentrations in experiments NAT11, S11 and SYN11 were similar to their calculated equilibrium values (Table 2). The similar behavior of natural versus

synthetic gypsum further confirms the generality of the results obtained in this study.

5.3 Geochemical modeling of experimental results and retrieval of reaction rates

The results of this study are well adapted for quantification using geochemical modeling. To a first approximation, we assume that the rates of gypsum dissolution is controlled by detachment of material from its surface consistent with transition-state-theory (TST) in accord with (Aagaard and Helgeson, 1982; Lasaga, 1984):

$$r = k_{gp} S \prod_i a_i^{n_i} \exp\left(-\frac{E_a}{RT}\right) f(\Delta G_R) \quad (10)$$

where the r refers to the dissolution rate, k_{gp} stands for a dissolution rate constant, S denotes the reactive surface area of the mineral in the fluid, a denotes the activity of species i , and the exponent n_i represents a reaction order (Lasaga et al., 1994; Oelkers et al., 1994), E_a signifies an apparent activation energy, R symbolizes the gas constant, and T stands for absolute temperature. The dimensionless term $f(\Delta G_R)$ is a function of the distance from the thermodynamic equilibrium with respect to the dissolving phase and is given by:

$$f(\Delta G_R) = [1 - \exp(\Delta G_R / RT)]^{q_i} \quad (11)$$

where ΔG_R designates the free energy of the reaction – a review of the development of this rate equation is provided by (Lasaga et al., 1981). The term q_i refers to an empirical parameter, which was found to equal or close to 1 by most of the published studies on gypsum dissolution. To model the observed release rates of Ca^{2+} and SO_4^{2-} we adopted $q_i = 1.2$, as recommended for gypsum by Jeschke et al. (2001).

Calcite was chosen to be the only precipitating phase in the system for the model calculations, although there is visual evidence for the precipitation and subsequent dissolution of other calcium carbonate phases. This simplification was adopted for two reasons 1) kinetic parameters describing the precipitation of vaterite and to a lesser degree aragonite are lacking in the literature, and 2) calcite is the most stable carbonate phase detected in this study (Katz et al., 1972; Rao, 1973; Spanos and Koutsoukos, 1998; Bots et al., 2012; Rodriguez-Navarro et al., 2015; Rodriguez-Blanco et al., 2011, 2017). Taking account to the combined processes of nucleation and growth, calcite

precipitation rates can be described using Combining the BCF growth equation with a simplified form of Eqn. (11), where the nucleation rate parameters are grouped into the single constant Γ , the following equation can be deduced describing calcite precipitation rates (Walton et al., 1967; Nielsen, 1983; Shiraki and Brantley, 1995; Pham et al., 2011; Hellevang et al., 2013):

$$r_- = -k_- S \prod_i a_i^{n_i} \exp\left(-\frac{E_a}{RT}\right) \{\Omega - 1\}^2 - k_N \exp\left\{-\Gamma \left(\frac{1}{(T)^{3/2} \ln \Omega}\right)^2\right\}, \quad (12)$$

where the precipitation rate constant k_- was taken to be equal to $1.0 \times 10^{-7.06}$ as reported by Naviaux et al. (2019) and values of k_N and Γ were respectively set to either 1 or 2 mol/s and 2.0×10^{10} in agreement with the values recommended by Pham et al. (2011) for calcite nucleation. Note that Eqn. (12) is based on the assumption that calcite nucleates on a specific substrate; in this study all secondary carbonates are observed to nucleate on the surfaces of the dissolving gypsum. The calcite reactive surface area S during the precipitation was estimated using

$$S = A_{Cc} \cdot M \cdot n \quad (13)$$

where A_{Cc} designates the specific area of calcite, M refers to the molar weight and n stands for the number of moles of calcite. The specific surface area, A_{Cc} , in Eqn. (13) cannot be determined independently, so were determined by a fit of the experimental data.

Rate equations (10) and (12) were incorporated into PHREEQC to calculate the chemical evolution of the experiments performed in this study. Modelling of the experimental data was conducted iteratively by the progressive reduction of the difference between measured and modeled Ca and S concentrations and pH. The results of these regression calculations are shown in Fig. 4 - 6, where a close correspondence can be seen between the experimental results and the model calculations. The model results in this figure are consistent with a gypsum rate constant (k_{gp}) of $1.1 \pm 0.1 \times 10^{-7}$ mol/m²/s. Note that there are only minor differences between measured and modeled solution pH's, the latter being lower by no more than 0.4 units compared to the measurements. Such a discrepancy may be within the accuracy of the model calculation but may be also due to the uncertainty of the thermodynamic constants for the carbonate

system or to partial exchange of the experimental solutions with atmosphere CO₂. In addition, it must be emphasized that calcite was not the only Ca-carbonate phase observed in the post-reaction solids. As shown in Figs. 8, vaterite, and possibly some ACC, were also identified among the reaction products.

A good agreement is also found between experimentally measured and calculated CaCO₃ content of the solids recovered after the experiments. As showed in Table 5, the difference between the CaCO₃ contents deduced from total carbon (TIC) measurements and those calculated from the PHREEQC model is within $\pm 5\%$.

The gypsum dissolution rates generated in this study are significantly lower than those reported by several studies in the literature. For instance, [Jeschke et al. \(2001\)](#) reported a gypsum dissolution rate constant k of 1.3×10^{-3} mol/m²/s at near to neutral pH, whereas [Colombani \(2008\)](#) reported values ranging between 3 and 7×10^{-5} mol/m²/s based also on a review of previous work. A recent study by [Feng et al. \(2017\)](#) on the dissolution of gypsum (010) cleavage surface by digital holographic microscopy reported an average dissolution flux of 3.0×10^{-6} mol/m²/s in deionized water. The wide range of rate constant values reported in the literature likely stems from different factors including: the origin and grain size of sample powders, the experimental approach, the influence of hydrodynamic conditions and the type of functions used to regress the data (cf. [Jeschke and Dreybrodt, 2002](#); [Colombani, 2008](#); [Tang et al. 2018](#)). Even so, the rates of gypsum dissolution found in the present study are significantly slower than those reported by other studies. Although no studies of gypsum dissolution in alkaline and carbonate-rich solution have been published, it is possible that the reaction is strongly inhibited under these conditions, as observed for some silicate minerals (e.g., [Xie, 1994](#); [Pokrovsky and Schott, 2000](#)).

5.4. Implications for carbon storage

The results presented above suggest that gypsum carbonation will be rapid if this mineral is present in the subsurface and the reaction thermodynamically favored (e.g. at basic pH conditions - see Fig. 1). Moreover, the precipitation of CaCO₃ at gypsum surfaces was found not to inhibit its dissolution process. Similar rapid carbonation was

found in past studies for CaCO₃ minerals replacing gypsum, anhydrite and bassanite (Karkanas, 2010; Petrash et al., 2012; Schultheiss et al., 2013; Ruiz-Agudo et al., 2015; González-Illanes et al., 2017). The transformation of gypsum to Ca-carbonate changes the volume of the solid phase. The density of calcite is 0.027 mol/cm³ whereas the densities of gypsum and anhydrite are 0.013 mol/cm³ and 0.022 mol/cm³, respectively. As such as gypsum transforms into calcite significant pore space will be created (Fernández-Díaz et al., 2009; González-Illanes et al., 2017). Consequently, the gypsum-calcite transformation could potentially provide migration channels, promoting further carbonation or increasing the possibility of CO₂ loss from the storage reservoir. A similar although smaller volume decrease occurs from the transformation of anhydrite to calcite. If the goal of a subsurface carbon injection is the carbonation of a gypsum or anhydrite bearing evaporite deposit, the volume change brought about by the dissolution of gypsum or anhydrite and precipitation of calcite would favor efficient mineral storage if sufficient alkalinity was available to continue favoring this transformation. Note, however, that during the coupled gypsum dissolution Ca-carbonate precipitation (reaction 5) protons are produced, which will tend to destabilize calcite over time. In contrast, if a subsurface carbon storage site was designed to retain injected CO₂ with the aid of an evaporite caprock, the opening of pore space via reaction 5 could prove problematical allowing CO₂ to escape towards the surface.

Some CO₂ capture and storage efforts have proposed to use seawater to capture CO₂ and use the resulting gas-charged water to carbonate sub-seafloor basalts (McGrail et al., 2006; Goldberg et al., 2008; Wolff-Boenisch et al., 2011). As seawater contains substantial aqueous sulfate, the first calcium-bearing phase to precipitate in the basalt due to this injection prior to the neutralization of the injected water by basalt dissolution could be either gypsum or anhydrite (c.f. Voigt et al., 2018). The precipitation of gypsum or anhydrite would occur because the carbonic acid in the gas-charged seawater would trigger the dissolution of basaltic rock, which produces aqueous Ca²⁺. Alternatively, if the target storage reservoir was at temperatures in excess of ~150 °C anhydrite might precipitate directly from heating the CO₂ charged seawater (Bischoff and Dickson, 1975; Voigt et al., 2018). The results of this study demonstrate that if

gypsum or anhydrite forms during the early stages of CO₂ storage in sub-sea floor basalt, it might not limit calcite precipitation over the long-term. Once sufficient basalt dissolved, the pH would increase, destabilizing gypsum and promoting calcite precipitation (Fig. 1). The results presented above confirm that this reaction is rapid and can occur on timescales of hours.

6. CONCLUSIONS

This study investigated the carbonation of gypsum in closed-system reactors. The results demonstrate the rapid and efficient carbonation of gypsum at those pH conditions where this reaction is thermodynamically favored. Indeed, the experimental results show that at close to equilibrium conditions are attained between gypsum and calcite within days. These results have significant consequences for subsurface mineral carbonation efforts. Consideration of the thermodynamic stability of these phases, such as shown in Fig. 1, the presence of gypsum and anhydrite in evaporite cap rocks might be expected to rapidly carbonate if in the presence of aqueous carbonate at pH > 5.0 to 7.5 depending on at CO₂ partial pressure. As the gypsum to calcite reaction is volume negative, these reactions will tend to damage the caprock potentially provoking CO₂ leakage. The carbonation of gypsum, however, if present in submarine basalts could enhance carbon storage in these systems.

Acknowledgments

We would like to thank Gary Tarbuck, James Davy and Haiye Yu for their technical support. We are also grateful for the help and insights that Ian Wood offered on the XRD analyses. We also like to thank Floris Teuling, Ron Mulders and Lisa Füllenbach for their helpful discussions. This project has received funding from the European Union's Horizon 2020 research and innovation programme under the Marie Skłodowska-Curie grant agreement No 675219.

REFERENCES

- Aagaard, P., Helgeson, H.C., 1982. Thermodynamic and kinetic constraints on reaction rates among minerals and aqueous solutions; I, Theoretical considerations. *282(3)*: 237-285.
- Ahr, W.M., 2008. *Geology of carbonate reservoirs: the identification, description and characterization of hydrocarbon reservoirs in carbonate rocks*. John Wiley & Sons.
- Alfredsson, H.A., Hardarson, B.S., Franzson, H., Gislason, S.R., 2008. CO₂ sequestration in basaltic rock at the Hellisheidi site in SW Iceland: stratigraphy and chemical composition of the rocks at the injection site. *Mineralogical Magazine*, 72(1): 1-5.
- Altree-Williams, A., Pring, A., Ngothai, Y., Brugger, J., 2017. The Carbonation of Anhydrite: Kinetics and Reaction Pathways. *ACS Earth and Space Chemistry* 1, 89-100.
- Anadón, P., Rosell, L., Talbot, M.R., 1992. Carbonate replacement of lacustrine gypsum deposits in two Neogene continental basins, eastern Spain. *Sedimentary Geology*, 78(3): 201-216.
- Azdarpour, A., Asadullah, M., Junin, R., Manan, M., Hamidi, H., Mohammadian, E., 2014. Direct carbonation of red gypsum to produce solid carbonates. *Fuel Processing Technology* 126, 429-434.
- Bachu, S., Gunter, W., Perkins, E., 1994. Aquifer disposal of CO₂: hydrodynamic and mineral trapping. *Energy Conversion and management*, 35(4): 269-279.
- Baines, S.J., Worden, R.H., 2004. The long-term fate of CO₂ in the subsurface: natural analogues for CO₂ storage. Geological Society, London, Special Publications, 233(1): 59-85.
- Benson, S.M., Cole, D.R., 2008. CO₂ Sequestration in Deep Sedimentary Formations. *Elements*, 4(5): 325-331.
- Bischoff, J., 1968. Catalysis, inhibition, and the calcite-aragonite problem; [Part] 2, The vaterite-aragonite transformation. *American Journal of Science* 266, 80-90.
- Bischoff, J.L., Fyfe, W., 1968. Catalysis, inhibition, and the calcite-aragonite problem; [Part] 1, The aragonite-calcite transformation. *American Journal of Science* 266, 65-79.
- Bischoff, J.L., Dickson, F.W., 1975. Seawater-basalt interaction at 200 °C and 500 bars: Implications for origin of sea-floor heavy-metal deposits and regulation of seawater chemistry. *Earth and Planetary Science Letters*, 25(3): 385-397.
- Bolze, J., Peng, B., Dingenouts, N., Panine, P., Narayanan, T., Ballauff, M., 2002. Formation and Growth of Amorphous Colloidal CaCO₃ Precursor Particles as Detected by Time-Resolved SAXS. *Langmuir* 18, 8364-8369.
- Bots, P., Benning, L.G., Rodriguez-Blanco, J.-D., Roncal-Herrero, T., Shaw, S., 2012. Mechanistic Insights into the Crystallization of Amorphous Calcium Carbonate

- (ACC). *Crystal Growth & Design*, 12(7): 3806-3814.
- Brečević, L., Nielsen, A.E., 1989. Solubility of amorphous calcium carbonate. *Journal of Crystal Growth*, 98(3): 504-510.
- Brunauer, S., Emmett, P.H., Teller, E., 1938. Adsorption of Gases in Multimolecular Layers. *Journal of the American Chemical Society* 60, 309-319.
- Burton, W.K., Cabrera, N., Frank, F.C., Mott Nevill, F., 1951. The growth of crystals and the equilibrium structure of their surfaces. *Philosophical Transactions of the Royal Society of London. Series A, Mathematical and Physical Sciences*, 243(866): 299-358.
- Christoffersen, J.R., Christoffersen, M.R., 1976. The kinetics of dissolution of calcium sulphate dihydrate in water. *Journal of Crystal Growth* 35, 79-88.
- Cizer, Ö., Rodriguez-Navarro, Carlos., Ruiz-Agudo, E., Elsen, J., Van Gemert, D., Van Balen, K., 2012a. Phase and morphology evolution of calcium carbonate precipitated by carbonation of hydrated lime. *Journal of Materials Science*, 47(16): 6151-6165.
- Cizer, Ö., Van Balen, K., Elsen, J., Van Gemert, D., 2012b. Real-time investigation of reaction rate and mineral phase modifications of lime carbonation. *Construction and Building Materials*, 35: 741-751.
- Colombani, J., Bert, J., 2007. Holographic interferometry study of the dissolution and diffusion of gypsum in water. *Geochimica et Cosmochimica Acta* 71, 1913-1920.
- Colombani, J., 2008. Measurement of the pure dissolution rate constant of a mineral in water. *Geochimica et Cosmochimica Acta*, 72(23): 5634-5640.
- Feng, P., Brand, A.S., Chen, L., Bullard, J.W., 2017. In situ nanoscale observations of gypsum dissolution by digital holographic microscopy. *Chemical Geology* 460, 25-36.
- Fernández-Díaz, L., Pina, C.M., Astilleros, J.M., Sánchez-Pastor, N., 2009. The carbonation of gypsum: Pathways and pseudomorph formation. *American Mineralogist* 94, 1223-1234.
- Fernández-Díaz, L., Putnis, A., Prieto, M., Putnis, C.V., 1996. The role of magnesium in the crystallization of calcite and aragonite in a porous medium. 66(3): 482-491.
- Flaathen, T.K., Gislason, S.R., Oelkers, E.H., Sveinbjörnsdóttir, Á.E., 2009. Chemical evolution of the Mt. Hekla, Iceland, groundwaters: A natural analogue for CO₂ sequestration in basaltic rocks. *Applied Geochemistry*, 24(3): 463-474.
- Galeczka, I., Wolff-Boenisch, D., Oelkers, E.H., Gislason, S.R., 2014. An experimental study of basaltic glass–H₂O–CO₂ interaction at 22 and 50 °C: Implications for subsurface storage of CO₂. *Geochimica et Cosmochimica Acta*, 126: 123-145.
- García, M., Dávila, G., Offeddu, F., Soler, J.M., Cama, J., 2011. Reactions during CO₂ geological sequestration: dissolution of calcite and dolomite coupled to gypsum precipitation. *Rev. Soc. Esp. Mineral*, 2: 93-94.

- Gislason, S.R., Wolff-Boenisch, D., Stefansson, A., Oelkers, E.H., Gunnlaugsson, E., Sigurdardottir, H., Sigfusson, B., Broecker, W.S., Matter, J.M., Stute, M., Axelsson, G., Fridriksson, T., 2010. Mineral sequestration of carbon dioxide in basalt: A pre-injection overview of the CarbFix project. *International Journal of Greenhouse Gas Control*, 4(3): 537-545.
- Gislason, S.R., Oelkers, E.H., 2014. Carbon Storage in Basalt. *Science*, 344(6182): 373-374.
- Given, R.K., Wilkinson, B.H., 1985. Kinetic control of morphology, composition, and mineralogy of abiogenic sedimentary carbonates. *Journal of Sedimentary Research*, 55(1): 109-119.
- Goldberg, D., Aston, L., Bonneville, A., Demirkanli, I., Evans, C., Fisher, A., Garcia, H., Gerrard, M., Heesemann, M., Hnottavange-Telleen, K., Hsu, E., Malinverno, C., Moran, K., Park, A.A., Scherwath, M., Slagle, A., Stute, M., Weathers, T., Webb, R., White, M., White S., 2018. Geological storage of CO₂ in sub-seafloor basalt: the CarbonSAFE pre-feasibility study offshore Washington State and British Columbia. *Energy Procedia*, 146: 158-165.
- Goldberg, D.S., Takahashi, T., Slagle, A.L., 2008. Carbon dioxide sequestration in deep-sea basalt. *105(29)*: 9920-9925.
- González-Illanes, T., Borrero, M.T., Herráez, M.M., Pimentel, C., Pina, C.M., 2017. Pseudomorphic replacement of Mg–Ca Carbonates after gypsum and anhydrite. *ACS Earth and Space Chemistry* 1, 168-178.
- Gudbrandsson, S., Wolff-Boenisch, D., Gislason, S.R., Oelkers, E.H., 2011. An experimental study of crystalline basalt dissolution from $2 \leq \text{pH} \leq 11$ and temperatures from 5 to 75°C. *Geochimica et Cosmochimica Acta*, 75(19): 5496-5509.
- Gunter, W., Wiwehar, B., Perkins, E., 1997. Aquifer disposal of CO₂-rich greenhouse gases: extension of the time scale of experiment for CO₂-sequestering reactions by geochemical modelling. *Mineralogy and Petrology*, 59(1-2): 121-140.
- Hangx, S.J.T., Christopher, J.S., Colin, J.P., 2010. Mechanical behavior of anhydrite caprock and implications for CO₂ sealing capacity. *Journal of Geophysical Research: Solid Earth* 115.B7.
- Hellevang, H., Pham, V.T.H., Aagaard, P., 2013. Kinetic modelling of CO₂-water-rock interactions. *International Journal of Greenhouse Gas Control*, 15: 3-15.
- IPCC (2005) Underground geological storage. In: Metz, B., Davidson, O., De Coninck, H., (eds) IPCC Special Report on Carbon Dioxide Capture and Storage, prepared by Working Group III of the Intergovernmental Panel on Climate Change. Cambridge University Press, Cambridge, UK, and New York, USA, pp 195-276
- Jeschke, A.A., Vosbeck, K., Dreybrodt, W., 2001. Surface controlled dissolution rates of gypsum in aqueous solutions exhibit nonlinear dissolution kinetics. *Geochimica et Cosmochimica Acta* 65, 27-34.

- Jeschke, A.A., Dreybrodt, W., 2002. Pitfalls in the determination of empirical dissolution rate equations of minerals from experimental data and a way out: an iterative procedure to find valid rate equations, applied to Ca-carbonates and -sulphates. *Chemical Geology*, 192(3): 183-194.
- Johnson, J., Anderson, G., Parkhurst, D., 2000. Database "thermo.com.V8.R6.230." Lawrence Livermore National Laboratory, Livermore, California, USA.
- Johnson, J.W., Nitao, J.J., Steefel, C.I., Knauss, K.G., 2001. Reactive Transport Modeling of Geologic CO₂ Sequestration in Saline Aquifers: The Influence of Intra-Aquifer Shales and the Relative Effectiveness of Structural, Solubility, and Mineral Trapping During Prograde and Retrograde Sequestration, Lawrence Livermore National Lab., CA (US).
- Karkanias, P., 2010. Preservation of anthropogenic materials under different geochemical processes: A mineralogical approach. *Quaternary International* 214, 63-69.
- Katz, A., Sass, E., Starinsky, A., Holland, H.D., 1972. Strontium behavior in the aragonite-calcite transformation: An experimental study at 40 - 98 °C. *Geochimica et Cosmochimica Acta*, 36(4): 481-496.
- Lackner, K.S., Wendt, C.H., Butt, D.P., Joyce, E.L., Sharp, D.H., 1995. Carbon dioxide disposal in carbonate minerals. *Energy*, 20(11): 1153-1170.
- Lackner, K.S., 2003. A guide to CO₂ sequestration. *Science*, 300(5626), 1677-1678.
- Lasaga, A.C., 1984. Chemical kinetics of water-rock interactions. *Journal of Geophysical Research: Solid Earth*, 89(B6): 4009-4025.
- Lasaga, A.C. (1981) Rate laws of chemical reactions. *Reviews in Mineralogy*, 8, 1-68.
- Lasaga, A.C., Soler, J.M., Ganor, J., Burch, T.E., Nagy, K.L., 1994. Chemical weathering rate laws and global geochemical cycles. *Geochimica et Cosmochimica Acta*, 58(10): 2361-2386.
- Lee, M.g., Jang, Y.N., Ryu, K.W., Kim, W., Bang, J.H., 2012. Mineral carbonation of flue gas desulfurization gypsum for CO₂ sequestration. *Energy* 47, 370-377.
- Liu, S.T., Nancollas, G.H., 1971. The kinetics of dissolution of calcium sulfate dihydrate. *Journal of Inorganic and Nuclear Chemistry* 33, 2311-2316.
- Marini, L., 2006. Geological Sequestration of Carbon Dioxide: Thermodynamics, Kinetics, and Reaction Path Modeling. *Developments in Geochemistry*, vol. 11. Elsevier.
- Matter, J.M., Broecker, W.S., Gislason, S.R., Gunnlaugsson, E., Oelkers, E.H., Stute, M., Sigurdardóttir, H., Stefansson, A., Alfredsson, H.A., Aradóttir, E.S., Axelsson, G., Sigfússon, B., Wolff-Boenisch, D., 2011. The CarbFix Pilot Project-Storing carbon dioxide in basalt. *Energy Procedia*, 4: 5579-5585.
- Matter, J.M., Stute, M., Snæbjörnsdóttir, S.Ó., Oelkers, E.H., Gislason, S.R., Aradóttir, E.S., Sigfússon, B., Gunnarsson, I., Sigurdardóttir, H., Gunnlaugsson, E., Axelsson,

- G., Alfredsson, H.A., Wolff-Boenisch, D., Mesfin, K., Taya, D.F., Hall, J., Dideriksen, K., Broecker, W.S., 2016. Rapid carbon mineralization for permanent disposal of anthropogenic carbon dioxide emissions. *Science*, 352(6291): 1312-1314.
- McGrail, B.P., Schaef, H.T., Ho, A.M., Chien, Y., Dooley, J.J., Davidson, C.L., 2006. Potential for carbon dioxide sequestration in flood basalts. *Journal of Geophysical Research: Solid Earth*, 111(B12).
- Moorehead, D.R., 1986. Cementation by the carbonation of hydrated lime. *Cement and Concrete Research*, 16(5): 700-708.
- Naviaux, J.D., Subhas, A.V., Rollins, N.E., Dong, S., Berelson, W.M., Adkins, J.F., 2019. Temperature dependence of calcite dissolution kinetics in seawater. *Geochimica et Cosmochimica Acta*, 246: 363-384.
- Nielsen, A.E., 1983. Precipitates: formation, coprecipitation, and aging. In: Kolthoff, I.M., Elving, P.J. (Eds.), *Treatise on Analytical Chemistry*. Wiley, pp. 269–347.
- Oelkers, E.H., Butcher, R., Pogge von Strandmann, P.A.E., Schuessler, J.A., Von Blanckenburg, F., Snæbjörnsdóttir, S.Ó., Mesfin, K., Aradóttir, E.S., Gunnarsson, I., Sigfússon, B., 2019. Using stable Mg isotope signatures to assess the fate of magnesium during the in situ mineralisation of CO₂ and H₂S at the CarbFix site in SW-Iceland. *Geochimica et Cosmochimica Acta*, 245: 542-555.
- Oelkers, E.H., Cole, D.R., 2008. Carbon dioxide sequestration a solution to a global problem. *Elements*, 4(5): 305-310.
- Oelkers, E.H., Gislason, S.R., Matter, J., 2008. Mineral Carbonation of CO₂. *Elements*, 4(5): 333-337.
- Oelkers, E.H., Schott, J., 2005. Geochemical aspects of CO₂ sequestration. *Chemical Geology*, 217(3-4): 183-186.
- Oelkers, E.H., Schott, J., Devidal, J.L., 1994. The effect of aluminum, pH, and chemical affinity on the rates of aluminosilicate dissolution reactions. *Geochimica et Cosmochimica Acta*, 58(9): 2011-2024.
- Olsson, J., Stipp, S.L.S., Makovicky, E., Gislason, S.R., 2014. Metal scavenging by calcium carbonate at the Eyjafjallajökull volcano: A carbon capture and storage analogue. *Chemical Geology*, 384: 135-148.
- Pacala, S., Socolow, R., 2004. Stabilization Wedges: Solving the Climate Problem for the Next 50 Years with Current Technologies. *Science*, 305(5686): 968.
- Palandri, J.L., Kharaka, Y.K., 2004. A compilation of rate parameters of water-mineral interaction kinetics for application to geochemical modeling, Geological Survey Menlo Park CA.
- Parkhurst, D.L., Appelo, C., 2013. Description of input and examples for PHREEQC version 3 - A computer program for speciation, batch-reaction, one-dimensional transport, and inverse geochemical calculations.

- Peckmann, J., Paul, J., Thiel, V., 1999. Bacterially mediated formation of diagenetic aragonite and native sulfur in Zechstein carbonates (Upper Permian, Central Germany). *Sedimentary Geology*, 126(1): 205-222.
- Pérez-Moreno, S.M., Gázquez, M.J., Bolívar, J.P., 2015. CO₂ sequestration by indirect carbonation of artificial gypsum generated in the manufacture of titanium dioxide pigments. *Chemical Engineering Journal* 262, 737-746.
- Petrash, D.A., Gingras, M.K., Lalonde, S.V., Orange, F., Pecoits, E., Konhauser, K.O., 2012. Dynamic controls on accretion and lithification of modern gypsum-dominated thrombolites, Los Roques, Venezuela. *Sedimentary Geology* 245-246, 29-47.
- Pham, V.T.H., Lu, P., Aagaard, P., Zhu, C., Hellevang, H., 2011. On the potential of CO₂-water-rock interactions for CO₂ storage using a modified kinetic model. *International Journal of Greenhouse Gas Control*, 5(4): 1002-1015.
- Pogge von Strandmann, P.A.E., Burton, K.W., James, R.H., Van Calsteren, P., Gislason, S.R., 2010. Assessing the role of climate on uranium and lithium isotope behaviour in rivers draining a basaltic terrain. *Chemical Geology*, 270(1): 227-239.
- Pokrovsky, O.S., Schott, J., 2000. Kinetics and mechanism of forsterite dissolution at 25 °C and pH from 1 to 12. *Geochimica et Cosmochimica Acta* 64, 3313-3325.
- Pontoni, D., Bolze, J., Dingenouts, N., Narayanan, T., Ballauff, M., 2003. Crystallization of Calcium Carbonate Observed In-situ by Combined Small- and Wide-angle X-ray Scattering. *The Journal of Physical Chemistry B* 107, 5123-5125.
- Power, I.M., Harrison, A.L., Dipple, G.M., Wilson, S.A., Kelemen, P.B., Hitch, M., Southam, G., 2013. Carbon mineralization: from natural analogues to engineered systems. *Reviews in Mineralogy and Geochemistry*, 77(1): 305-360.
- Putnis, A., 2009. Mineral Replacement Reactions. *Reviews in Mineralogy and Geochemistry*, 70(1): 87-124.
- Rahmani, O., 2018. CO₂ sequestration by indirect mineral carbonation of industrial waste red gypsum. *Journal of CO₂ Utilization* 27, 374-380.
- Rao, M.S., 1973. Kinetics and Mechanism of the Transformation of Vaterite to Calcite. *Bulletin of the Chemical Society of Japan*, 46(5): 1414-1417.
- Rendel, P.M., Gavrieli, I., Wolff-Boenisch, D., Ganor, J., 2016. Gypsum solubility under pressure conditions relevant to CO₂ geological storage. *International Journal of Greenhouse Gas Control*, 55: 15-22.
- Rodriguez-Blanco, J.D., Shaw, S., Benning, L.G., 2011. The kinetics and mechanisms of amorphous calcium carbonate (ACC) crystallization to calcite, via vaterite. *Nanoscale*, 3(1): 265-271.
- Rodriguez-Navarro, C., Kudłacz, K., Cizer, Ö., Ruiz-Agudo, E., 2015. Formation of amorphous calcium carbonate and its transformation into mesostructured calcite.

CrystEngComm, 17(1): 58-72.

- Roncal-Herrero, T., Astilleros, J.M., Bots, P., Rodríguez-Blanco, J.D., Prieto, M., Benning, L.G., Fernández-Díaz, L., 2017. Reaction pathways and textural aspects of the replacement of anhydrite by calcite at 25 °C. *American Mineralogist* 102, 1270-1278.
- Rodríguez-Blanco, J.D., Sand, K.K., Benning, L.G., 2017. ACC and Vaterite as Intermediates in the Solution-Based Crystallization of CaCO₃. In: Van Driessche, A.E.S., Kellermeier, M., Benning, L.G., Gebauer, D. (Eds.), *New Perspectives on Mineral Nucleation and Growth: From Solution Precursors to Solid Materials*. Springer International Publishing, Cham, pp. 93-111.
- Rodríguez-Blanco, J.D., Shaw, S., Benning, L.G., 2011. The kinetics and mechanisms of amorphous calcium carbonate (ACC) crystallization to calcite, via vaterite. *Nanoscale*, 3(1): 265-271.
- Rodríguez-Navarro, C., Kudłacz, K., Cizer, Ö., Ruiz-Agudo, E., 2015. Formation of amorphous calcium carbonate and its transformation into mesostructured calcite. *CrystEngComm*, 17(1): 58-72.
- Ruiz-Agudo, E., Putnis, C.V., Hövelmann, J., Álvarez-Lloret, P., Ibañez-Velasco, A., Putnis, A., 2015. Experimental study of the replacement of calcite by calcium sulphates. *Geochimica et Cosmochimica Acta*, 156: 75-93.
- Ruiz-Agudo, E., Putnis, C.V., Hövelmann, J., Álvarez-Lloret, P., Ibañez-Velasco, A., Putnis, A., 2015. Experimental study of the replacement of calcite by calcium sulphates. *Geochimica et Cosmochimica Acta* 156, 75-93.
- Santos, R.M., Mertens, G., Salman, M., Cizer, Ö., Van Gerven, T., 2013. Comparative study of ageing, heat treatment and accelerated carbonation for stabilization of municipal solid waste incineration bottom ash in view of reducing regulated heavy metal/metalloid leaching. *Journal of Environmental Management*, 128: 807-821.
- Sawada, K., 1997. The mechanisms of crystallization and transformation of calcium carbonates. *Pure and Applied Chemistry*, 69(5): 921-928.
- Schaef, H.T., McGrail, B.P., Owen, A.T., 2009. Basalt-CO₂-H₂O interactions and variability in carbonate mineralization rates. *Energy Procedia*, 1(1): 4899-4906.
- Schaef, H.T., McGrail, B.P., Owen, A.T., 2010. Carbonate mineralization of volcanic province basalts. *International Journal of Greenhouse Gas Control*, 4(2): 249-261.
- Schrag, D.P., 2007. Preparing to Capture Carbon. *Science*, 315(5813): 812.
- Schultheiss, S., Sethmann, I., Schlosser, M., Kleebe, H.J., 2013. Pseudomorphic transformation of Ca/Mg carbonates into phosphates with focus on dolomite conversion, *Mineralogical Magazine*, p. 2725.
- Seo, S.K., Kim, Y., Chu, Y.S., Cho, H.K., 2018. Experimental Study of the Carbonation Properties of Dry Desulfurized Gypsum. *J. Korean Ceram. Soc* 55, 44-49.
- Shikazono, N., Harada, H., Ikeda, N., Kashiwagi, H., 2009. Dissolution of basaltic

rocks and its application to underground sequestration of CO₂-Estimate of mineral trapping by dissolution-precipitation simulation. *Japanese Magazine of Mineralogical and Petrological Sciences*, 38: 149-160.

- Shiraki, R., Brantley, S.L., 1995. Kinetics of near-equilibrium calcite precipitation at 100°C: An evaluation of elementary reaction-based and affinity-based rate laws. *Geochimica et Cosmochimica Acta*, 59(8): 1457-1471.
- Smith, M.M., Sholokhova, Y., Hao, Y., Carroll, S.A., 2012. Evaporite caprock integrity: an experimental study of reactive mineralogy and pore-scale heterogeneity during brine-CO₂ exposure. *Environ Sci Technol*, 47(1): 262-8.
- Snæbjörnsdóttir, S.Ó., Oelkers, E.H., Mesfin, K., Aradóttir, E.S., Dideriksen, K., Gunnarsson, I., Gunnlaugsson, E., Matter, J.M., Stute, M., Gislason, S.R., 2017. The chemistry and saturation states of subsurface fluids during the in situ mineralisation of CO₂ and H₂S at the CarbFix site in SW-Iceland. *International Journal of Greenhouse Gas Control*, 58: 87-102.
- Snæbjörnsdóttir, S.Ó., Gislason, S.R., Galeczka, I.M., Oelkers, E.H., 2018. Reaction path modelling of in-situ mineralisation of CO₂ at the CarbFix site at Hellisheidi, SW-Iceland. *Geochimica et Cosmochimica Acta*, 220: 348-366.
- Song, K., Jang, Y., Kim, W., Lee, M.G., Shin, D., Bang, J., Jeon, C.W., Chae, S.C., 2014. Factors affecting the precipitation of pure calcium carbonate during the direct aqueous carbonation of flue gas desulfurization gypsum. *Energy*, 65: 527-532.
- Spanos, N., Koutsoukos, P.G., 1998. The transformation of vaterite to calcite: effect of the conditions of the solutions in contact with the mineral phase. *Journal of Crystal Growth* 191, 783-790.
- Spencer, R.J., 2000. Sulfate minerals in evaporite deposits. *Reviews in Mineralogy and Geochemistry*, 40(1): 173-192.
- Stafford, K.W., Ulmer-Scholle, D., Rosales-lagarde, L., 2008. Hypogene calcite: Evaporite diagenesis in the western Delaware Basin. *Carbonates and Evaporites*, 23: 89-103.
- Stefánsson, A., Arnórsson, S., Gunnarsson, I., Kaasalainen, H., Gunnlaugsson, E., 2011. The geochemistry and sequestration of H₂S into the geothermal system at Hellisheidi, Iceland. *Journal of Volcanology and Geothermal Research*, 202(3): 179-188.
- Tan, W., Zhang, Z., Li, H., Li, Y., Shen, Z., 2017. Carbonation of gypsum from wet flue gas desulfurization process: experiments and modeling. *Environmental Science and Pollution Research* 24, 8602-8608.
- Tang, J., Bullard, J.W., Perry, L.N., Feng, P., Liu, J., 2018. An empirical rate law for gypsum powder dissolution. *Chemical Geology* 498, 96-105.
- Voigt, M., Pearce, C.R., Baldermann, A., Oelkers, E.H., 2018. Stable and radiogenic strontium isotope fractionation during hydrothermal seawater-basalt interaction. *Geochim. Cosmochim. Acta* 240, 131-151.

- Wakahama, H. Mitoa, S., Ohsumi, T., Ueda, A., Yajima, T., Satoh, H., Sugiyama, K., Ozawa, A., Ajima, S., Todaka, N., 2009. A concept of CO₂ Georeactor sequestration at the Ogachi HDR site, NE Japan. 1(1): 3683-3689.
- Walton, A.G., Füredi, H., Elving, P.J., Kolthoff, I.M., 1967. The formation and properties of precipitates, 23. Interscience Publishers New York.
- Wolff-Boenisch, D., Wenau, S., Gislason, S.R., Oelkers, E.H., 2011. Dissolution of basalts and peridotite in seawater, in the presence of ligands, and CO₂: Implications for mineral sequestration of carbon dioxide. *Geochimica et Cosmochimica Acta*, 75(19): 5510-5525.
- Xie Z., 1994. Surface properties of silicates, their solubility and dissolution kinetics. Ph. D. thesis, Northwestern University.

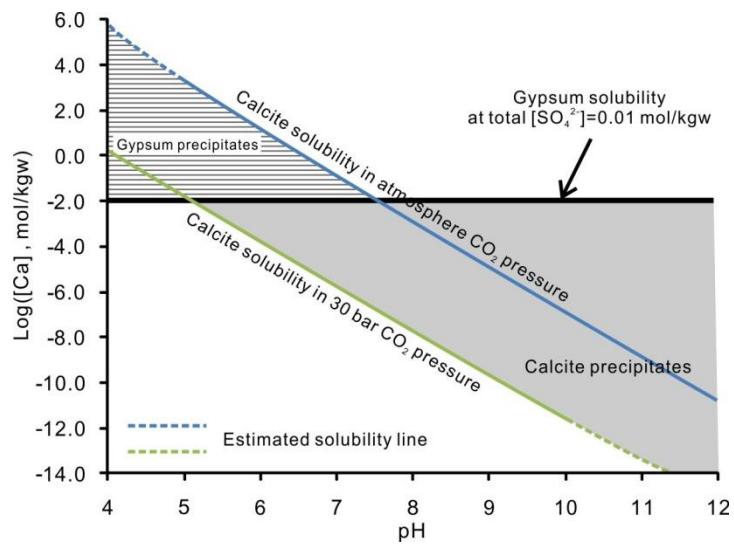


Figure 1. Calculated values of the logarithm of calcite solubility and logarithm of gypsum solubility in aqueous solutions having a total $[\text{SO}_4^{2-}] = 0.01 \text{ mol/kgw}$ and a total NaCl concentration of 0.01 mol/kgw versus fluid pH under atmosphere and 30 bar CO_2 partial pressure.

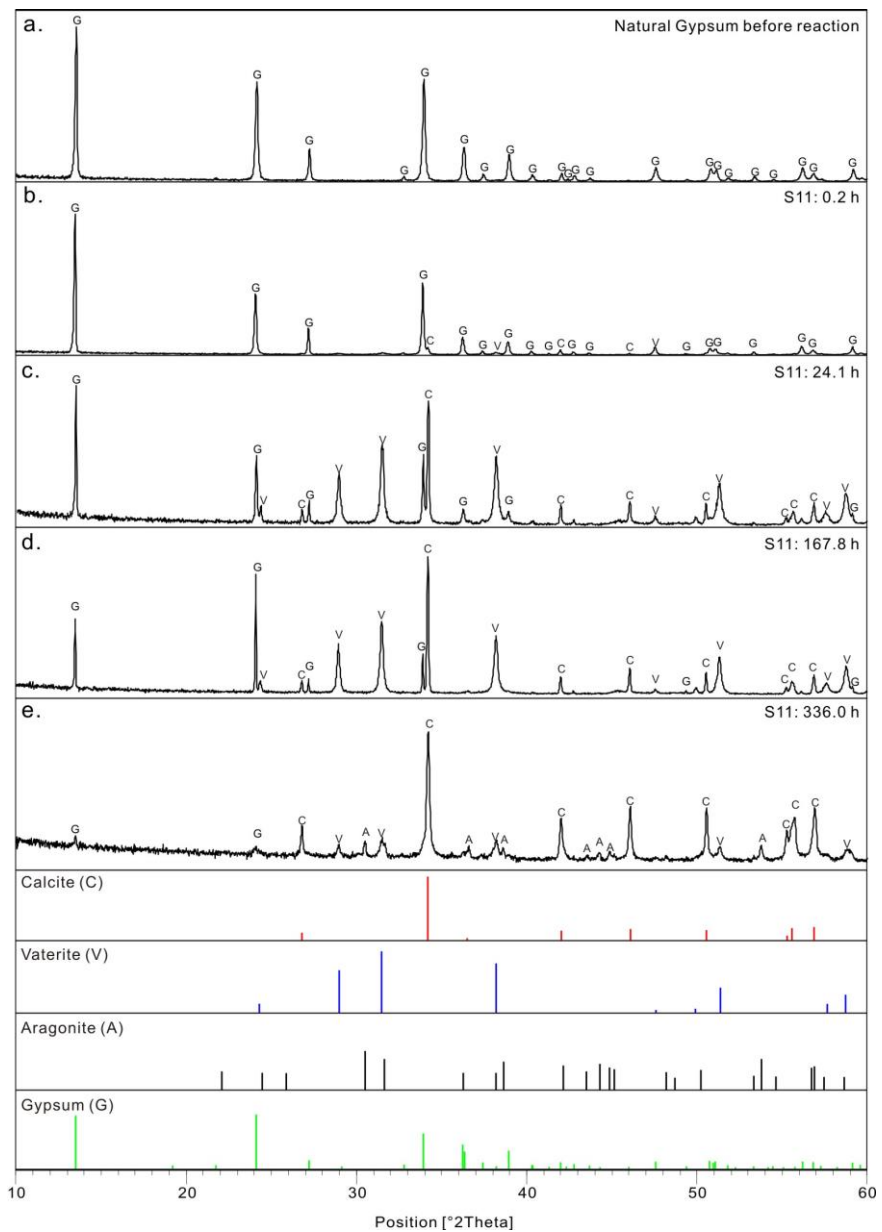


Figure 2. XRD diffractograms for solid samples before (a) and during experimental series S11 after (b) 0.2 h, (c) 24 h, (d) 167 h, and (e) 336 h. The XRD pattern of selected minerals are provided at the bottom of the figure for reference.

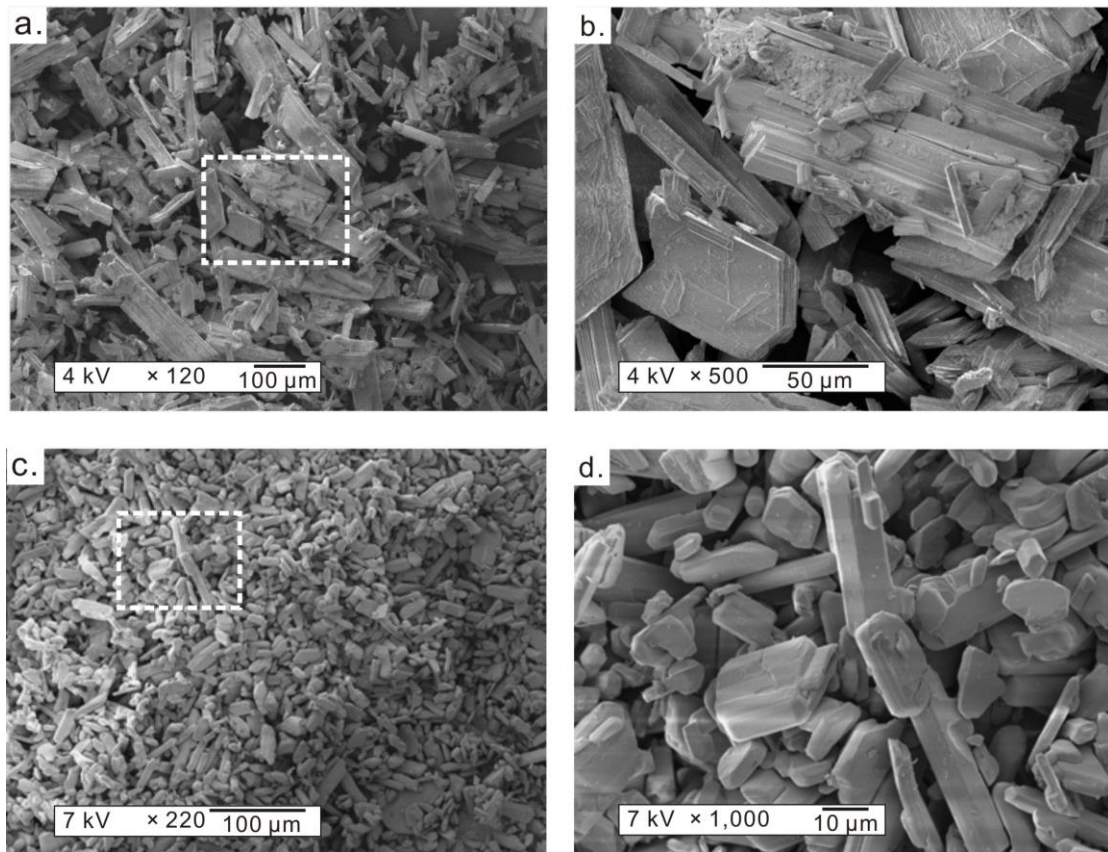


Figure 3. SEM images of the natural gypsum and synthetic gypsum used in this study. (a) natural gypsum before the experiments; (b) the magnified picture of dashed area in (a); (c) synthetic gypsum before the experiment; (d) the magnified picture of dashed area in (c).

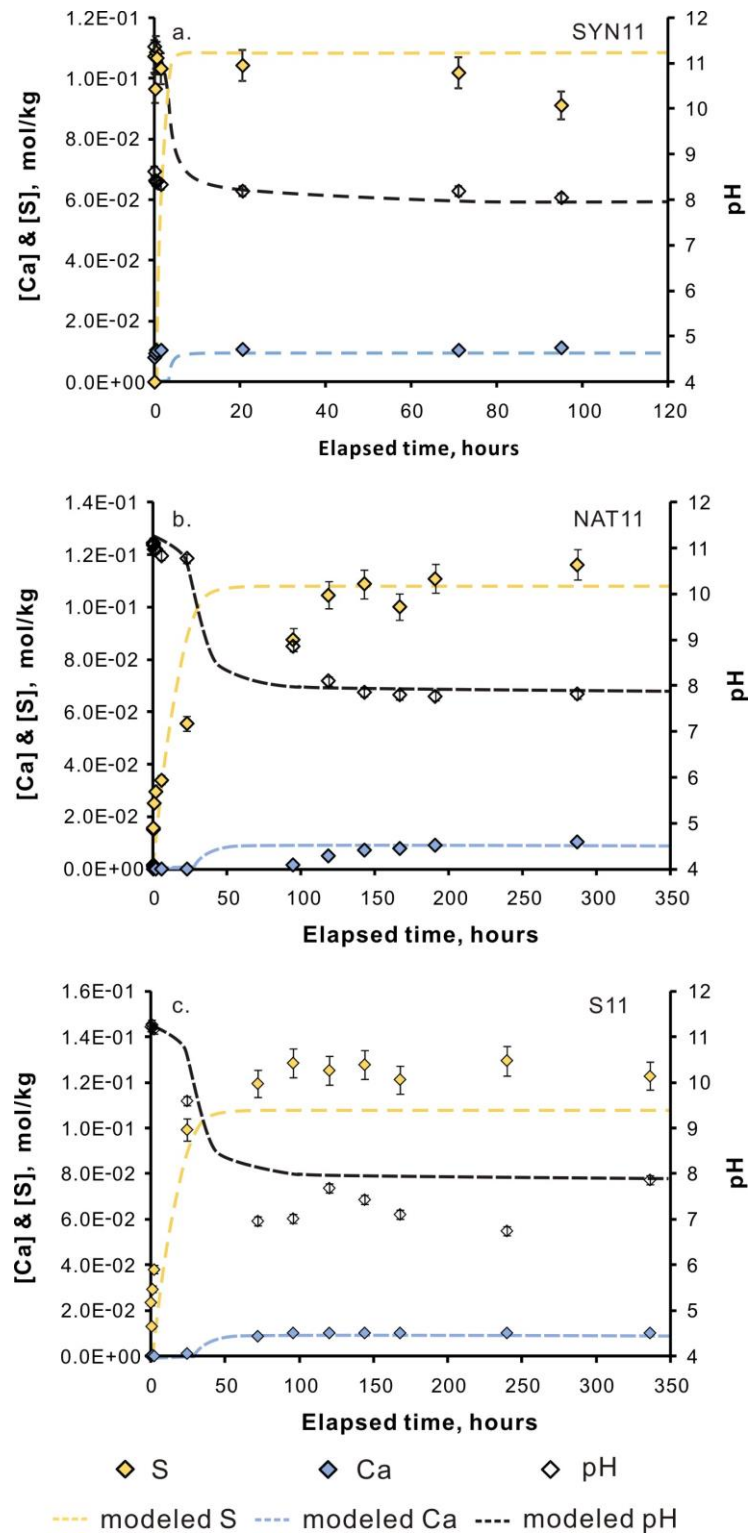


Figure 4. The evolution of dissolved S and Ca concentration and pH in the reactive fluid as a function of time: (a) experiment SYN11; (b) experiment NAT11 and (c) experimental series S11. The errors are smaller than the symbols unless otherwise shown.

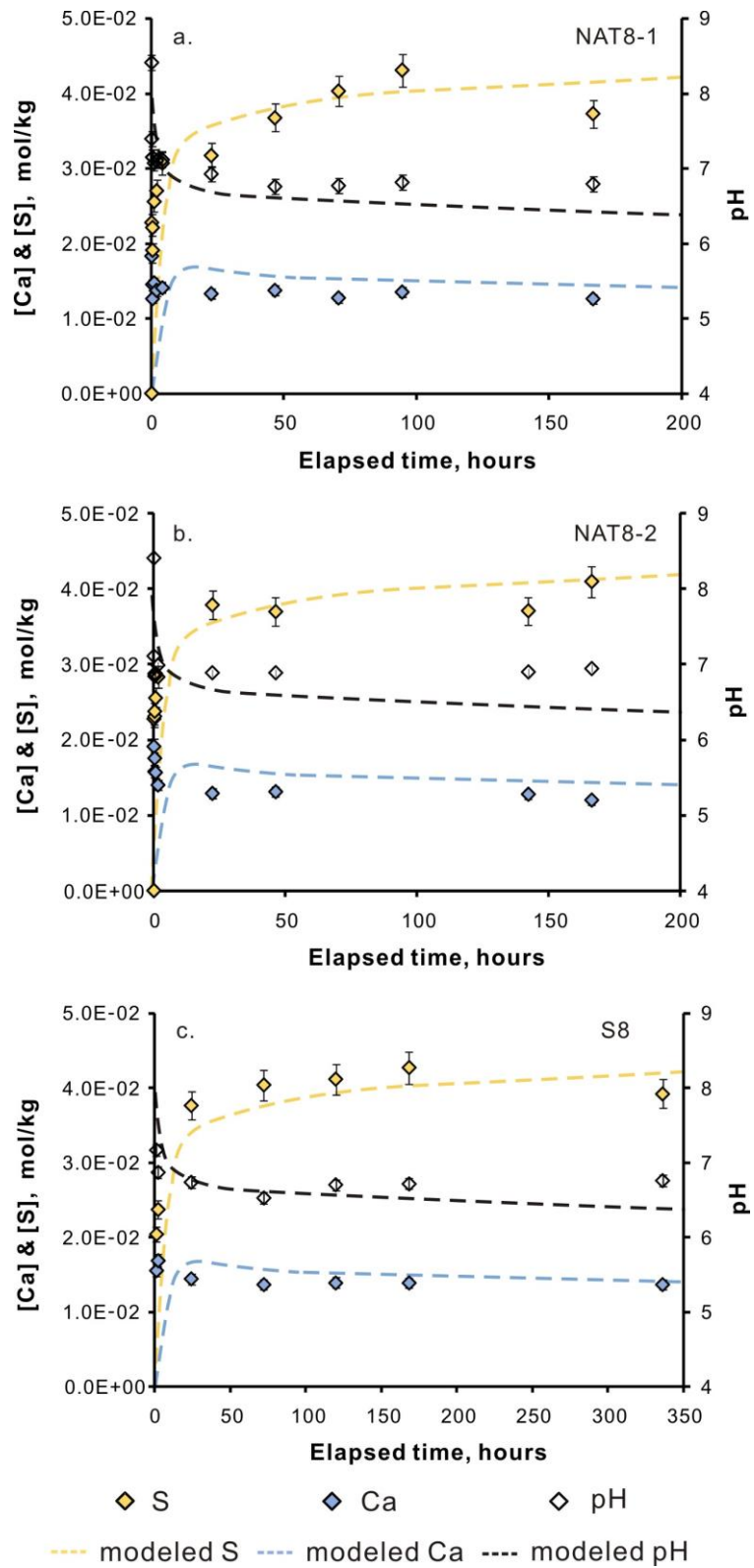


Figure 5. The evolution of dissolved S and Ca concentration and pH in the reactive fluid as a function of time for experiments (a) NAT8-1 and (b) NAT8-2, and (c) experimental series S8. The errors are smaller than the symbols unless otherwise shown.

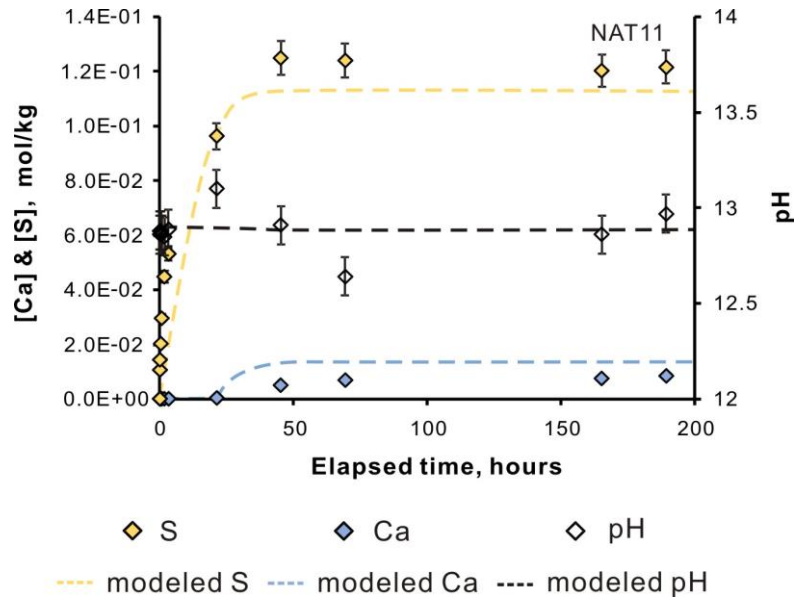
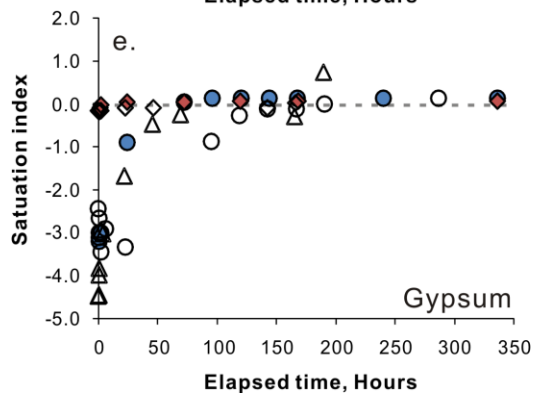
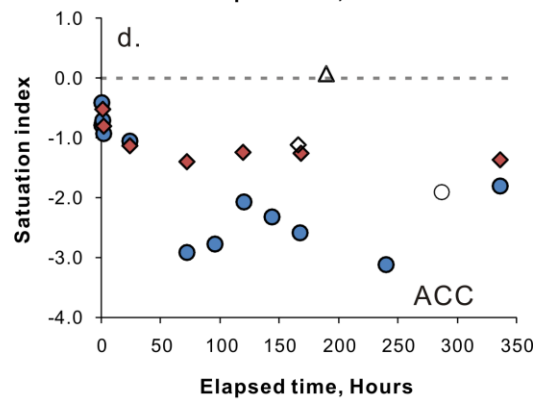
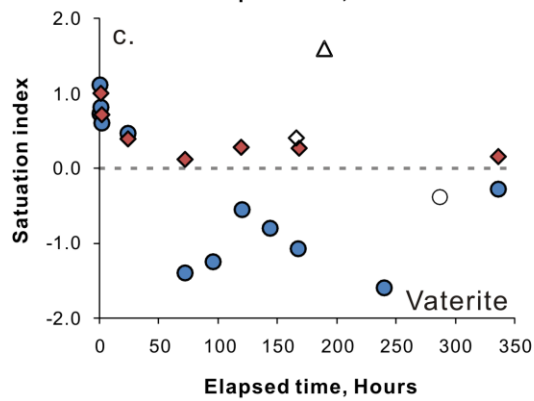
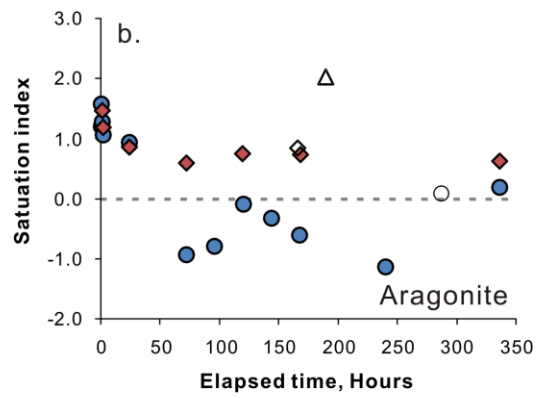
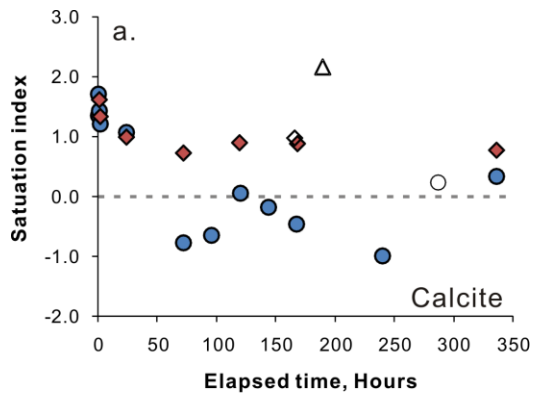


Figure 6. The evolution of dissolved S and Ca concentration and pH in the reactive fluid as a function of time for experiment NAT13. The errors are smaller than the symbols unless otherwise shown.



- S11
- NAT11
- ◆ S8
- ◇ NAT8-2
- △ NAT13

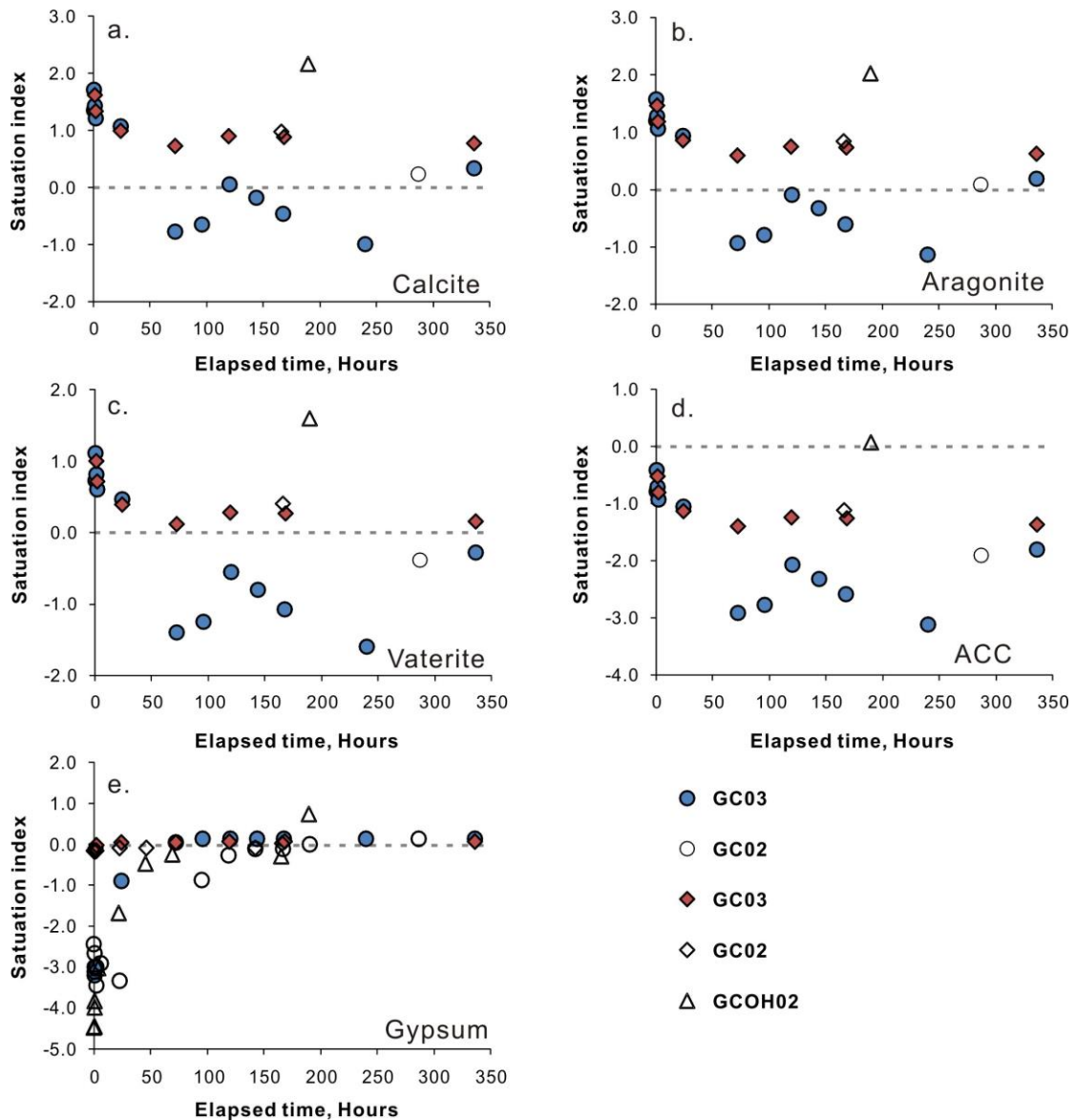


Figure 7. Calculated saturation indexes for carbonate minerals and gypsum in the reaction fluids of (a) calcite; (b) aragonite; (c) vaterite; (d) ACC; (e) gypsum. The error bars are based on variation between the duplicate experiments. The errors are smaller than the symbols unless otherwise shown.

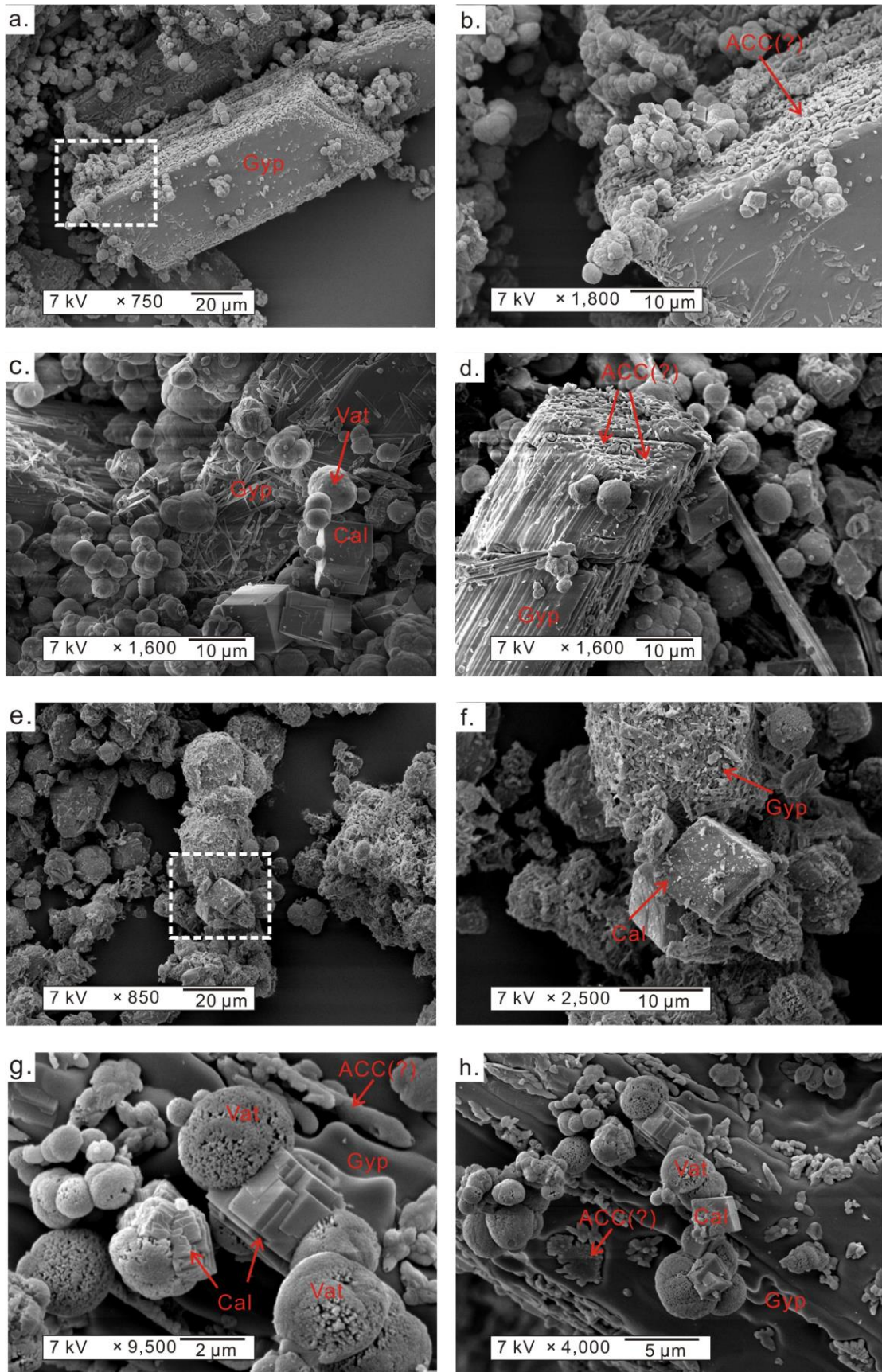


Figure 8. SEM images of the natural gypsum of the experimental series S11. (a) ACC, vaterite and calcite formed in the etch pits on the surface of gypsum (experiment S11-

1, reaction time: 0.2 h); (b) the magnified image of the dashed area in (a); (c) image showing vaterite and calcite on gypsum and hair-like gypsum dissolved remnants (experiment S11-3, reaction time: 1 h); (d) solids recovered from experiment S11-4, after 2h reaction time; (e) solids recovered from experiment S11-12 after 336.0 h of reaction time; (f) the magnified image of the dashed area in the picture (e). (g), (h) the transformation of vaterite into calcite during experimental series S11 after 0.2 h elapsed time. Note that the abbreviations ACC, Vat, Cal, and Gyp refer to amorphous calcium carbonate, vaterite, calcite, and gypsum, respectively.

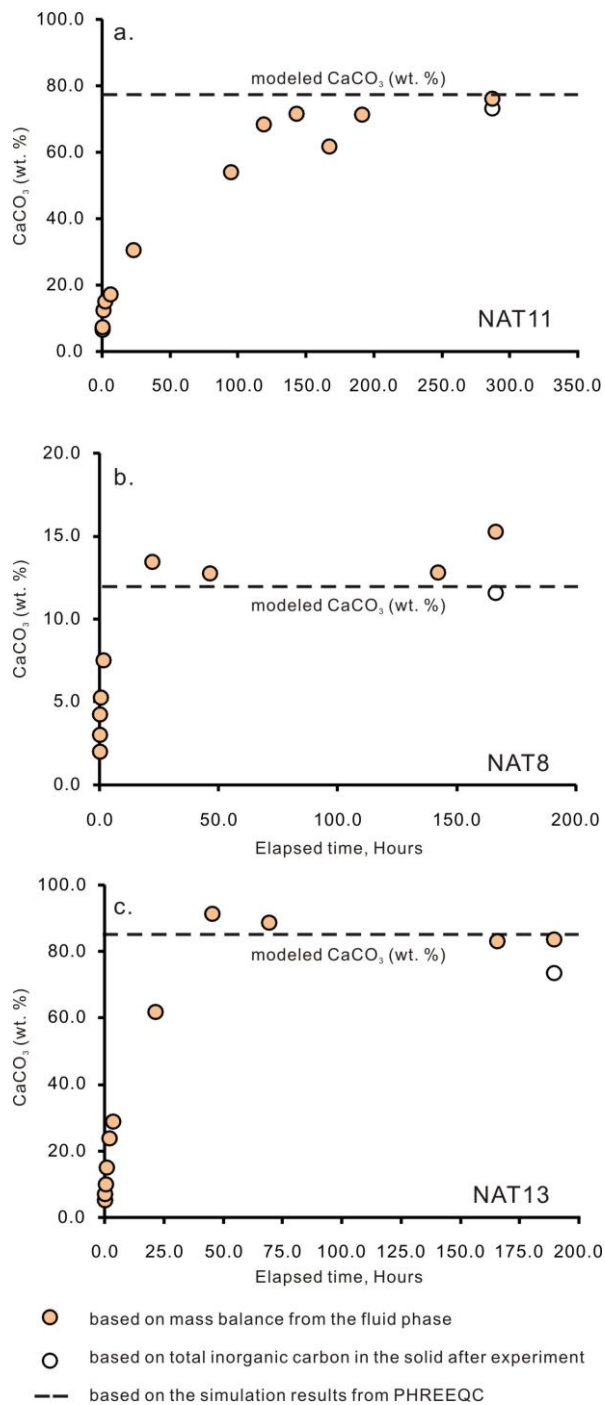


Figure 9. Temporal evolution of CaCO_3 content of the solids based on either 1) fluid phase mass balance calculations, 2) direct total inorganic carbon (TIC) measurements of the solids, and 3) the calculated possible maximum mass fraction of CaCO_3 based on PHREEQC model. (a) Experiment NAT11, (b) experiment NAT8-2, and (c) experiment NAT13 – see text.

Table 1. Summary of the experimental conditions of the batch experiments.

Experimental run	Gypsum type	Mixing method	Elapsed time h	Na ₂ CO ₃ mol/kgw	NaHCO ₃ mol/kgw	NaOH mol/kgw	pH	Gypsum mass g	Fluid mass G	Rock / Fluid ratio g / 100 g fluid
SYN11	Synthetic	Stir bar	94.9	0.1	/	/	11.36	4.80	226.3	2.12
NAT11	Natural	Shaking bath	286.8	0.1	/	/	11.11	4.80	224.3	2.14
S11-1	Natural	Shaking bath	0.2	0.1	/	/	11.30	1.40	72.10	1.94
S11-2	Natural	Shaking bath	0.6	0.1	/	/	11.42	1.40	71.70	1.95
S11-3	Natural	Shaking bath	1.0	0.1	/	/	11.42	1.40	71.29	1.97
S11-4	Natural	Shaking bath	2.0	0.1	/	/	11.42	1.40	72.23	1.94
S11-5	Natural	Shaking bath	24.1	0.1	/	/	11.42	1.40	72.64	1.93
S11-6	Natural	Shaking bath	71.9	0.1	/	/	11.30	1.40	70.67	1.98
S11-7	Natural	Shaking bath	96.1	0.1	/	/	11.35	1.40	70.43	1.99
S11-8	Natural	Shaking bath	120.1	0.1	/	/	11.35	1.40	70.82	1.98
S11-9	Natural	Shaking bath	144.1	0.1	/	/	11.29	1.40	71.41	1.96
S11-10	Natural	Shaking bath	167.8	0.1	/	/	11.29	1.40	70.63	1.98
S11-11	Natural	Shaking bath	240.0	0.1	/	/	11.35	1.40	70.48	1.99
S11-12	Natural	Shaking bath	336.0	0.1	/	/	11.37	1.40	71.58	1.96
NAT8-1	Synthetic	Stir bar	166.6	/	0.1	/	8.41	4.800	218.090	2.20
NAT8-2	Natural	Shaking bath	166.3	/	0.1	/	8.41	4.800	219.820	2.18
S8-1	Natural	Shaking bath	1.1	/	0.1	/	8.26	1.401	71.310	1.97
S8-2	Natural	Shaking bath	2.0	/	0.1	/	8.26	1.401	72.802	1.92
S8-3	Natural	Shaking bath	24.3	/	0.1	/	8.26	1.401	70.982	1.97
S8-4	Natural	Shaking bath	71.9	/	0.1	/	8.05	1.401	69.847	2.01
S8-5	Natural	Shaking bath	119.9	/	0.1	/	8.25	1.401	70.704	1.98
S8-6	Natural	Shaking bath	168.1	/	0.1	/	8.26	1.401	70.907	1.98

S8-7	Natural	Shaking bath	336.0	/	0.1	/	8.10	1.401	71.526	1.96
NAT13	Natural	Shaking bath	189.4	0.1	/	0.2	12.86	4.801	223.980	2.14

Table 2. Summary of the results of the experiments performed in 0.1 mol/kgw Na₂CO₃ solution at 25 °C.

Sample_No.	Elapsed time	pH	Alkalinity	Ca	S	DIC	SI	SI	SI	SI	SI
	(h)		Eq/kgw	mmol/kgw	mmol/kgw	mmol/kgw	Calcite	Aragonite	Vaterite	ACC	Gypsum
SYN11-0	0.00	11.36	N/A	N/A	N/A	N/A	N/A	N/A	N/A	N/A	N/A
SYN11-1	0.08	8.63	N/A	7.98	107.3	N/A	N/A	N/A	N/A	N/A	-0.07
SYN11-2	0.25	8.42	N/A	9.30	96.63	N/A	N/A	N/A	N/A	N/A	-0.07
SYN11-3	0.42	8.39	N/A	10.50	108.7	N/A	N/A	N/A	N/A	N/A	0.04
SYN11-4	0.58	8.40	N/A	10.10	106.7	N/A	N/A	N/A	N/A	N/A	0.02
SYN11-5	1.6	8.33	N/A	10.46	103.2	N/A	N/A	N/A	N/A	N/A	0.01
SYN11-6	20.6	8.19	N/A	10.58	104.3	N/A	N/A	N/A	N/A	N/A	0.03
SYN11-7	71.0	8.19	N/A	10.50	101.9	N/A	N/A	N/A	N/A	N/A	0.01
SYN11-8	95.0	8.04	N/A	11.20	91.02	N/A	N/A	N/A	N/A	N/A	-0.01
NAT11	0.0	11.11	N/A	0.0057	0	N/A	N/A	N/A	N/A	N/A	N/A
NAT11-1	0.1	11.12	N/A	1.74	15.09	N/A	N/A	N/A	N/A	N/A	-2.44
NAT11-2	0.3	11.07	N/A	1.02	15.78	N/A	N/A	N/A	N/A	N/A	-2.65
NAT11-3	0.8	10.97	N/A	0.256	25.03	N/A	N/A	N/A	N/A	N/A	-3.00
NAT11-4	1.8	10.98	N/A	0.0756	29.66	N/A	N/A	N/A	N/A	N/A	-3.44
NAT11-5	5.8	10.84	N/A	0.206	34.04	N/A	N/A	N/A	N/A	N/A	-2.91
NAT11-6	22.8	10.77	N/A	0.0336	55.54	N/A	N/A	N/A	N/A	N/A	-3.35
NAT11-7	94.8	8.86	N/A	1.640	87.65	N/A	N/A	N/A	N/A	N/A	-0.88
NAT11-8	118.8	8.10	N/A	5.14	104.6	N/A	N/A	N/A	N/A	N/A	-0.26
NAT11-9	142.8	7.86	N/A	7.18	108.8	N/A	N/A	N/A	N/A	N/A	-0.11
NAT11-10	166.8	7.80	N/A	7.81	100.0	N/A	N/A	N/A	N/A	N/A	-0.11
NAT11-11	190.8	7.77	N/A	9.28	110.9	N/A	N/A	N/A	N/A	N/A	0.00
NAT11-12	286.8	7.82	0.0017	10.58	116.3	1.75	0.24	0.09	-0.38	-1.90	0.14
S11-1	0.2	11.22	0.1641	0.166	23.41	83.04	1.35	1.20	0.73	-0.79	-3.20

S11-2	0.6	11.27	0.1725	0.417	12.94	87.03	1.72	1.58	1.11	-0.41	-3.12
S11-3	1.0	11.20	0.1363	0.299	29.36	68.91	1.44	1.29	0.82	-0.70	-3.01
S11-4	2.0	11.16	0.1224	0.125	38.11	62.03	1.21	1.07	0.60	-0.92	-3.00
S11-5	24.1	9.60	0.0040	1.11	99.31	3.02	1.08	0.94	0.47	-1.05	-0.89
S11-6	71.9	6.97	0.0014	8.75	119.5	1.66	-0.78	-0.93	-1.40	-2.92	0.06
S11-7	96.1	7.01	0.0016	10.30	128.6	1.81	-0.64	-0.79	-1.25	-2.77	0.14
S11-8	120.1	7.68	0.0017	10.19	125.2	1.78	0.06	-0.09	-0.55	-2.07	0.13
S11-9	144.1	7.43	0.0017	10.30	127.8	1.84	-0.18	-0.33	-0.80	-2.32	0.14
S11-10	167.8	7.11	0.0019	10.21	121.2	2.13	-0.46	-0.60	-1.07	-2.59	0.13
S11-11	240.0	6.74	0.0013	10.36	129.5	1.70	-0.99	-1.13	-1.60	-3.12	0.14
S11-12	336.0	7.87	0.0021	10.23	122.9	2.11	0.34	0.19	-0.28	-1.80	0.13

Table 3. Summary of gypsum dissolution experiments performed in 0.1 mol/kgw NaHCO₃ solution at 25 °C.

Sample_No.	Elapsed	pH	Alkalinity Eq/kgw	Ca mmol/kgw	S mmol/kgw	DIC mmol/kgw	SI Calcite	SI Aragonite	SI Vaterite	SI ACC	SI Gypsum
	time (h)										
NAT8-1-0	0	8.41	N/A	0.0244	0.0497	N/A	N/A	N/A	N/A	N/A	N/A
NAT8-1-1	0.17	7.40	N/A	18.31	22.75	N/A	N/A	N/A	N/A	N/A	-0.16
NAT8-1-2	0.33	7.15	N/A	14.48	22.15	N/A	N/A	N/A	N/A	N/A	-0.24
NAT8-1-3	0.58	7.15	N/A	12.66	19.07	N/A	N/A	N/A	N/A	N/A	-0.35
NAT8-1-4	1.08	7.07	N/A	14.71	25.56	N/A	N/A	N/A	N/A	N/A	-0.18
NAT8-1-5	2.08	7.10	N/A	13.70	27.08	N/A	N/A	N/A	N/A	N/A	-0.18
NAT8-1-6	4.08	7.12	N/A	14.10	30.74	N/A	N/A	N/A	N/A	N/A	-0.12
NAT8-1-7	22.6	6.93	N/A	13.32	31.78	N/A	N/A	N/A	N/A	N/A	-0.13
NAT8-1-8	46.6	6.76	N/A	13.72	36.77	N/A	N/A	N/A	N/A	N/A	-0.06
NAT8-1-9	70.6	6.77	N/A	12.70	40.28	N/A	N/A	N/A	N/A	N/A	-0.06
NAT8-1-10	94.6	6.81	N/A	13.47	43.06	N/A	N/A	N/A	N/A	N/A	-0.01
NAT8-1-11	166.6	6.79	N/A	12.59	37.25	N/A	N/A	N/A	N/A	N/A	-0.09
NAT8-2-0	0.0	8.41	N/A	0.037	0.108	N/A	N/A	N/A	N/A	N/A	N/A
NAT8-2-1	0.1	7.11	N/A	19.15	22.79	N/A	N/A	N/A	N/A	N/A	-0.14
NAT8-2-2	0.2	6.88	N/A	17.54	23.14	N/A	N/A	N/A	N/A	N/A	-0.16
NAT8-2-3	0.3	6.85	N/A	15.80	23.76	N/A	N/A	N/A	N/A	N/A	-0.18
NAT8-2-4	0.7	6.88	N/A	15.68	25.63	N/A	N/A	N/A	N/A	N/A	-0.16
NAT8-2-5	1.7	6.99	N/A	14.05	28.32	N/A	N/A	N/A	N/A	N/A	-0.16
NAT8-2-6	22.3	6.89	N/A	12.93	37.89	N/A	N/A	N/A	N/A	N/A	-0.08
NAT8-2-7	46.3	6.89	N/A	13.15	37.01	N/A	N/A	N/A	N/A	N/A	-0.08
NAT8-2-8	142.3	6.90	N/A	12.79	37.07	N/A	N/A	N/A	N/A	N/A	-0.09
NAT8-2-9	166.3	6.95	0.044	12.03	40.97	51.64	0.98	0.84	0.41	-1.11	0.02

S8-1	1.1	7.17	0.067	15.59	20.40	74.36	1.62	1.47	1.00	-0.52	-0.09
S8-2	2.0	6.87	0.067	16.92	23.72	82.27	1.34	1.19	0.72	-0.80	-0.02
S8-3	24.3	6.74	0.056	14.41	37.67	73.40	1.00	0.86	0.39	-1.13	0.05
S8-4	71.9	6.53	0.052	13.70	40.40	77.92	0.73	0.59	0.12	-1.40	0.05
S8-5	119.9	6.70	0.050	13.92	41.14	67.13	0.90	0.75	0.28	-1.24	0.07
S8-6	168.1	6.72	0.048	13.89	42.72	62.96	0.88	0.74	0.27	-1.25	0.08
S8-7	336.0	6.76	0.031	13.65	39.24	40.40	0.78	0.63	0.16	-1.36	0.08

Table 4. Summary of the results of gypsum dissolution experiments performed in 0.1 mol/kgw NaHCO₃ + 0.2 mol/kgw NaOH solution at 25 °C.

Sample_No.	duration (h)	pH	Alkalinity (Eq/kgw)	Ca mmol/kgw	S mmol/kgw	DIC mmol/kgw	SI Calcite	SI Aragonite	SI Vaterite	SI ACC	SI Gypsum
NAT13	0	12.86	N/A	0.013	0.000	N/A	N/A	N/A	N/A	N/A	N/A
NAT13-1	0.1	12.88	N/A	0.027	10.49	N/A	N/A	N/A	N/A	N/A	-4.47
NAT13-2	0.3	12.88	N/A	0.020	14.31	N/A	N/A	N/A	N/A	N/A	-4.45
NAT13-3	0.5	12.88	N/A	0.038	20.28	N/A	N/A	N/A	N/A	N/A	-3.99
NAT13-4	0.9	12.86	N/A	0.035	29.69	N/A	N/A	N/A	N/A	N/A	-3.82
NAT13-5	1.9	12.85	N/A	0.155	44.85	N/A	N/A	N/A	N/A	N/A	-2.92
NAT13-6	3.4	12.89	N/A	0.107	53.29	N/A	N/A	N/A	N/A	N/A	-3.02
NAT13-7	21.4	13.10	N/A	0.454	96.28	N/A	N/A	N/A	N/A	N/A	-1.68
NAT13-8	45.4	12.91	N/A	5.00	124.8	N/A	N/A	N/A	N/A	N/A	-0.47
NAT13-9	69.4	12.64	N/A	6.85	123.9	N/A	N/A	N/A	N/A	N/A	-0.24
NAT13-10	165.4	12.86	N/A	7.50	120.2	N/A	N/A	N/A	N/A	N/A	-0.29
NAT13-11	189.4	12.97	0.158	8.48	121.5	1.38	2.17	2.03	1.60	0.08	0.74

Table 5. Summary of measured total inorganic carbon (TIC, wt. %) results and CaCO₃ (wt. %) in solid phase after experiment.

Solid No.	Reaction duration (h)	Measured TIC (wt. %)	Measured CaCO ₃ ¹ (wt. %)	Sequestration efficiency (g CO ₂ /g rock) ¹¹	Calculated CaCO ₃ ² (wt. %)	Calculated CaCO ₃ predicted on model (wt. %)
NAT11	286.8	9.781	65.1	0.322	76.2	77.5
NAT8-2	166.3	1.369	11.4	0.051	15.3	12.3
NAT13	189.4	8.936	74.5	0.323	83.5	82.6

1. The measured CaCO₃ (wt.%) was calculated by the from the measured TIC using:

$$\text{CaCO}_3(\text{wt. \%}) = \frac{\text{Measured Carbon (wt. \%)}}{M_{\text{Carbon}}} \times M_{\text{CaCO}_3}, \text{ where } M_{\text{carbon}} = 12.0107 \text{ g/mol}; M_{\text{CaCO}_3} = 100.09 \text{ g/mol.}$$

2. Calculated based on Eqn. (8) and Eqn. (9).